© 2021. Published by The Company of Biologists Ltd | Journal of Cell Science (2021) 134, jcs258948. doi:10.1242/jcs.258948

TOOLS AND RESOURCES

CZON-cutter – a CRISPR-Cas9 system for multiplexed organelle imaging in a simple unicellular alga

Naoto Tanaka[1], Yuko Mogi[1], Takayuki Fujiwara[2,3], Kannosuke Yabe[1], Yukiho Toyama[1], Tetsuya Higashiyama[1,4,5] and Yamato Yoshida[1,6,*]

ABSTRACT

The unicellular alga *Cyanidioschyzon merolae* has a simple cellular structure; each cell has one nucleus, one mitochondrion, one chloroplast and one peroxisome. This simplicity offers unique advantages for investigating organellar proliferation and the cell cycle. Here, we describe CZON-cutter, an engineered clustered, regularly interspaced, short palindromic repeats (CRISPR)/CRISPR-associated nuclease 9 (Cas9) system for simultaneous genome editing and organellar visualization. We engineered a *C. merolae* strain expressing a nuclear-localized Cas9–Venus nuclease for targeted editing of any locus defined by a single-guide RNA (sgRNA). We then successfully edited the algal genome and visualized the mitochondrion and peroxisome in transformants using fluorescent protein reporters with different excitation wavelengths. Fluorescent protein labeling of organelles in living transformants allows us to validate phenotypes associated with organellar proliferation and the cell cycle, even when the edited gene is essential. Combined with the exceptional biological features of *C. merolae*, CZON-cutter will be instrumental for investigating cellular and organellar division in a high-throughput manner.

This article has an associated First Person interview with the first author of the paper.

KEY WORDS: CRISPR-Cas9 gene editing, Multiplexed organelle imaging, Rhodophyta, *Cyanidioschyzon merolae*, Organelle division, Cell cycle

INTRODUCTION

Eukaryotic cells contain membrane-bound organelles, functionally specialized units that respond to intercellular and intracellular signals for homeostasis and provide separate compartments for the biosynthesis of various biochemicals in varied metabolic pathways. Mitochondria and chloroplasts (plastids) are surrounded by a double membrane and are thought to have evolved from endosymbiotic bacteria (Gray, 1992; Martin and Kowallik, 1999; Mereschkowsky, 1905). Because of their evolutionary origin, they have their own genomes and only multiply via binary fission of pre-existing copies according to their own division cycles (Gillham et al., 1994; Kobayashi et al., 2011; Kuroiwa et al., 1998; Suzuki et al., 1994). Whether (and how) the cellular, nuclear, mitochondrial and plastid division cycles cooperate in the cells of photosynthetic eukaryotes is still largely unknown.

To fill this gap in our knowledge, researchers have recently focused on the simple unicellular alga *Cyanidioschyzon merolae*, commonly called 'CZON' (Matsuzaki et al., 2004; Nozaki et al., 2007). *C. merolae* cells possess very few membrane-bound organelles; each cell has one nucleus, one mitochondrion, one plastid, one peroxisome, one Golgi body with two cisternae, a few vacuoles and a simple-shaped endoplasmic reticulum (ER). All organelles divide shortly before cell division and are then inherited by the daughter cells (Imoto et al., 2010). Progression through the cell cycle can also be highly synchronized by entraining cultures to light–dark cycles (Suzuki et al., 1994). Together with its simple cell structure, these features provide *C. merolae* cells with unique advantages for investigating the molecular mechanisms related to organellar and cellular proliferation, as well as the cell cycle.

A series of studies using *C. merolae* have identified key factors for mitochondrial division [mitochondrial FtsZ, dynamin 1 (DNM1) and MITOCHONDRION-DIVIDING RING1 (MDR1)] and for plastid division [plastid FtsZ, dynamin 2 (DNM2), and PLASTID-DIVIDING RING1 (PDR1)] (Miyagishima et al., 2003; Nishida et al., 2003; Takahara et al., 2000; Yoshida et al., 2010, 2017). A subgroup of the kinesin super family participates in chromosome segregation (Yoshida et al., 2013). Furthermore, a recent transcriptome analysis using synchronized *C. merolae* cultures identified 454 genes with an expression pattern driven by the cell cycle, of which 181 genes have no known function (Fujiwara et al., 2020). These unknown genes might contribute to organellar and cellular division.

Gene targeting approaches are indispensable and powerful tools to study the function of a gene. An optimized gene targeting technique has been established for *C. merolae* using homologous recombination (HR) and a positive selection method for uracil auxotrophy or chloramphenicol resistance (Fujiwara et al., 2013, 2017; Imamura et al., 2009; Minoda et al., 2004). However, HR-mediated deletion of a locus typically entails assembling a targeting construct consisting of 1-kb fragments specific for the target gene flanking the *URA5.3* selection marker before introduction into *C. merolae* cells (Fig. 1A). Even though *C. merolae* has a very small genome (16.5 Mb for the nuclear genome, encoding 4775 proteins; Matsuzaki et al., 2004; Nozaki et al., 2007), the time-consuming and labor-intensive process necessary for gene targeting has severely impeded genome-wide genetic analysis of *C. merolae*. The multi-step process of conventional gene targeting thus restricts investigation and

[1]Department of Biological Sciences, Graduate School of Science, The University of Tokyo, 7-3-1 Hongo, Bunkyo, Tokyo 113-0033, Japan. [2]Department of Gene Function and Phenomics, National Institute of Genetics, Mishima, Shizuoka 411-8540, Japan. [3]Department of Genetics, Graduate University for Advanced Studies, SOKENDAI, Mishima, Shizuoka 411-8540, Japan. [4]Division of Biological Science, Graduate School of Science, Nagoya University, Furo-cho, Chikusa-ku, Nagoya, Aichi 464-8602, Japan. [5]Institute of Transformative Bio-Molecules (WPI-ITbM), Nagoya University, Furo-cho, Chikusa-ku, Nagoya, Aichi 464-8601, Japan. [6]Japan Science and Technology Agency (JST), PRESTO, 7-3-1 Hongo, Bunkyo, Tokyo 113-0033, Japan.

*Author for correspondence (yamato.yoshida@bs.s.u-tokyo.ac.jp)

Y.Y., 0000-0002-2339-2938

Handling Editor: David Stephens
Received 23 May 2021; Accepted 27 September 2021

Journal of Cell Science (2021) 134, jcs258948. doi:10.1242/jcs.258948

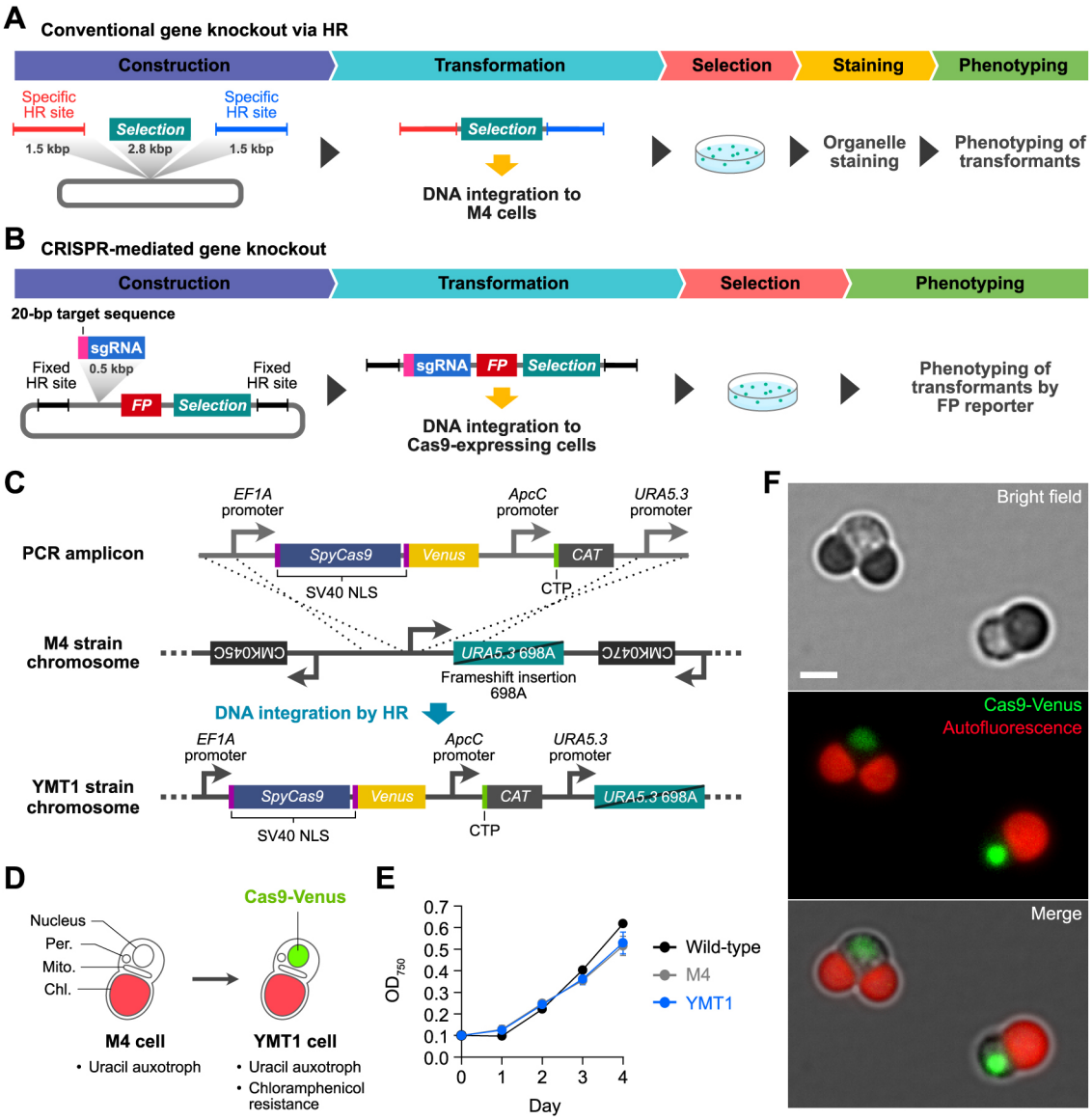

Fig. 1. Development of the *C. merolae* YMT1 strain expressing *Cas9-Venus*. (A) Schematic depiction of a conventional gene targeting approach using homologous recombination in *C. merolae*. (B) Schematic depiction of the CRISPR-mediated gene targeting system with simultaneous organelle visualization. (C) Schematic diagram of insertion of the *S. pyogenes Cas9* gene fused to *Venus* (*Cas9-Venus*) and the selection marker *CAT* into the safe harbor site by homologous recombination. PCR amplicon, introduced linear DNA; M4 strain chromosome, genomic structure of the parental uracil-auxotrophic M4 strain, with the HR integration site. YMT1 strain chromosome, structure of the inserted *Cas9-Venus* and *CAT* cassettes in *C. merolae* strain YMT1. The *Cas9-Venus* cassette includes a 1-kb fragment of the *EF1A* promoter and 278 bp of the *UBQ3* 3′ untranslated region (UTR) for constitutive expression. Cas9-Venus was fused to two copies of a nuclear localization sequence (NLS) from the SV40 T antigen to localize the Cas9-Venus fusion protein to the nucleus. *CAT* is driven by the constitutive *ApcC* promoter with transcription termination by the *TUBB* (β-tubulin) 3′ UTR. The *CAT* coding sequence is preceded by a chloroplast transit peptide (CTP). The complete amino acid sequence of Cas9-Venus is given in Table S5. (D) Schematic illustration of the *C. merolae* YMT1 strain. (E) Growth curves for the wild-type 10D, M4, and YMT1 strains. The 10D strain was cultured in 2× Allen's medium. M4 and YMT1 strains were cultured in 2× Allen's medium supplemented with uracil. Results are mean±s.d. (n=3 from cell culture replicates). (F) Imaging of a dividing cell (left) and a non-dividing cell (right) of *C. merolae* YMT1 strain. Green, Cas9-Venus fluorescence. Red, chlorophyll autofluorescence. Images are representative of more than five experiments. Scale bar: 2 µm.

is not efficient. Furthermore, organellar morphology should be characterized by live microscopy observations using fluorescently labeled organelles in the resulting knockout cells to determine whether the targeted gene is involved in cellular and/or organellar division. Therefore, a simpler and higher-throughput method to inactivate gene function in *C. merolae* is needed.

Targeted genome editing via clustered, regularly interspaced, short palindromic repeats (CRISPR) and CRISPR-associated nuclease 9 (Cas9) has revolutionized genetic analysis (Adli, 2018; Jiang and Doudna, 2017; Sander and Joung, 2014). The CRISPR-Cas9 system relies on the formation of a complex between Cas9 (most often from *Streptococcus pyogenes*) and a single-guide RNA (sgRNA) whose sequence is complementary to 20 nucleotides (nt) of a sequence within the target gene, followed by a short DNA motif [protospacer-adjacent motif (PAM) sequence; NGG] (Nishimasu et al., 2014) that cleaves the genome at the target site. The resulting double-strand break can then be repaired via nonhomologous end-joining (NHEJ) or homology-directed repair (HDR) pathways in nearly all organisms. NHEJ-mediated repair frequently introduces insertion/deletion mutations (indels) of various lengths, which

Journal of Cell Science (2021) 134, jcs258948. doi:10.1242/jcs.258948

disrupt the open reading frame. When provided with exogenously supplied donor DNA templates, the HDR machinery can modify the genome by introducing specific point mutations or inserting desired sequences at the target site. The CRISPR-Cas9 system has therefore become a powerful tool for targeted genome editing in many established and emerging model organisms.

Here, to identify genes that are involved in organellar and cellular division, we describe an engineered CRISPR-Cas9 system for *C. merolae*, named CZON-cutter, that allows simultaneous site-selective genome editing and multiplexed organellar imaging. This CRISPR-based gene targeting system can be used in the engineered *C. merolae* strain YMT1, which expresses *Cas9-Venus*, upon transformation with a PCR amplicon containing a designed sgRNA (Fig. 1B). Gene specificity can be achieved by altering the 20-nt target sequence of the sgRNA in the plasmid. Furthermore, the nucleus, the single mitochondrion, and the single peroxisome of transformed cells can be visualized by fluorescent protein reporters with different excitation wavelengths. The ability to image living transformants makes it possible to validate phenotypes associated with organellar morphology swiftly and accurately without chemical staining in the context of the cell cycle by time-lapse microscopy. The CZON-cutter platform thus holds great promise as an efficient, versatile, and high-throughput approach to investigate the biological function of any gene at organellar resolution.

RESULTS

Engineering of the *C. merolae* YMT1 strain expressing *Cas9-Venus* and a universal plasmid DNA template containing a sgRNA and a mitochondrial reporter

To implement the CZON-cutter platform in *C. merolae*, we first fused the coding sequence for *Cas9* from *S. pyogenes* to two copies of a nuclear localization sequence (*NLS*) and the yellow fluorescent protein gene *Venus*. Because the resulting *NLS-Cas9-NLS-Venus* construct is driven by the constitutive promoter from *ELONGATION FACTOR 1 ALPHA* (*EF1A*), Venus-tagged Cas9 (Cas9-Venus) should accumulate in the nucleus throughout the cell cycle. We then integrated a PCR amplicon consisting of the *Cas9-Venus* gene and a sequence encoding plastid-targeted chloramphenicol acetyltransferase (CAT) as a selectable marker into the region upstream of *URA5.3* in the *C. merolae* uracil-auxotrophic M4 strain by HR (Fig. 1C). The upstream region of *URA5.3* is one of the 'safe harbor' sites in the *C. merolae* genome, where integrations do not negatively affect the cell (Fujiwara et al., 2017; Kuroiwa et al., 2017). We selected transformants for resistance to chloramphenicol and named the resulting uracil-auxotrophic and chloramphenicol-resistant strain YMT1 (Fig. 1D). We confirmed that the YMT1 strain contains an inserted copy of the PCR amplicon and has a growth rate similar to that of the wild-type and M4 strains (Fig. 1E). Fluorescence microscopy of YMT1 cells specifically detected Venus fluorescence in the nucleus of dividing and non-dividing cells (Fig. 1F). We thus concluded that Cas9-Venus accumulates in the nucleus throughout the cell cycle.

Next, to edit the genome and visualize mitochondria simultaneously, we generated another construct with a sgRNA and a fluorescent mitochondrial marker in the region downstream of *Cas9-Venus* by HR. For greater versatility, we constructed a universal plasmid DNA template, pGuide-mitoScarlet, containing two homologous regions and gene cassettes for the sgRNA, the mitochondrion-targeted mScarlet marker gene (*mitoScarlet*) and the *URA5.3* selection marker (Fig. 2A). The sgRNA consisted of three segments: a 20-nt target-specific complementary region, a 76-nt scaffold region, and a 6-nt transcription termination signal (Fig. 2B). We placed the expression of the sgRNA under the control of a 593-bp promoter fragment from the *C. merolae* non-coding small nuclear RNA U6, which should be recognized by RNA polymerase III and thus be highly expressed in *C. merolae* cells. The cassette encoding the mitochondrion-targeted fluorescent protein comprised the coding sequence for the red fluorescent protein mitoScarlet fused to a mitochondrial targeting sequence (MTS) driven by the constitutive *CpcC* promoter derived from the 5′ untranslated region (UTR) of *CpcC* encoding phycocyanin-associated rod linker protein, followed by the *TUBB* (encoding β-Tubulin) 3′ UTR. This cassette was inserted into the plasmid downstream of *Venus* and upstream of *URA5.3*.

CRISPR-based genome editing in *C. merolae* is performed by the HDR pathway

To validate the CRISPR-Cas9 gene editing system described above with the YMT1 strain and the pGuide-mitoScarlet plasmid, we selected the putative cryptochrome gene *CRY* (also called *PHR1*, *C. merolae* Genome Project accession number, CMO348C) as a target for genome editing. Cryptochromes in the fruit fly *Drosophila melanogaster* and other insects act as blue light circadian photoreceptors and, in animals, they act as an integral component of the circadian machinery (Chaves et al., 2011; Öztürk et al., 2007), so we hypothesized that inactivation of *C. merolae CRY*, which clustered with animal and insect cryptochromes (Fig. S1), might disturb synchronization of cell division under light–dark cycles. Although the proteins encoded by the *C. merolae CRY* gene family exhibit photolyase activity, which can repair ultraviolet radiation-induced DNA damage, it remains unclear whether *C. merolae* CRYs behave as blue light photoreceptors (Asimgil and Kavakli, 2012).

We designed the sgRNA target sequence against *CRY* with the web tool CRISPRdirect (https://crispr.dbcls.jp/) (Naito et al., 2015) by selecting a unique target sequence with a very low possibility of off-target effects. We then attempted to integrate a PCR amplicon, using the resulting pGuide-$CRY_{232\text{-}254}$-mitoScarlet as template, into the genome of YMT1 cells by HR, but we failed to obtain a single positive genome-edited colony. This result suggests that *C. merolae* might not employ NHEJ to repair DNA double-strand breaks. In fact, the main components of the NHEJ pathway, *Ku70* and *Ku80* (Fell and Schild-Poulter, 2015), appear to be missing from the *C. merolae* genome.

Therefore, we next tested Cas9-mediated genome editing via the HDR pathway. We used single-stranded oligodeoxynucleotides (ssODNs) as a donor template, consisting of two homology arms of 30 nt each flanking the 20-nt *CRY* target sequence, which contained three single-base substitutions, one introducing a stop codon (CRY R79*) and the other two eliminating the PAM sequence in the *CRY* target region (Fig. 2C). We then transfected the YMT1 strain with a PCR amplicon corresponding to pGuide-mitoScarlet-CRY together with the ssODN to modify the target region of the *CRY* gene. We obtained 16 colonies by the uracil-autotrophic selection and 13 positive clones by sequencing (~11.1 transformants per 10^8 cells). As each positive clone contained several nucleotide substitutions in the *CRY* target region, we verified that Cas9-Venus-mediated mutations occurred in the target region of the 13 positive clones to evaluate accuracy and variation caused by unexpected mutations during genome editing (Fig. 2D–G). Ten clones (76.9%) harbored the desired mutations (Fig. 2D). The remaining three clones (23.1%) had imperfect and/or unexpected mutations at the *CRY* target site (Fig. 2E–G). Furthermore, we detected red fluorescence in mitochondria from the accumulation of mScarlet and green fluorescence from Cas9-Venus in all 13 colonies by fluorescence microscopy (Fig. 3A). These results demonstrated successful

Journal of Cell Science (2021) 134, jcs258948. doi:10.1242/jcs.258948

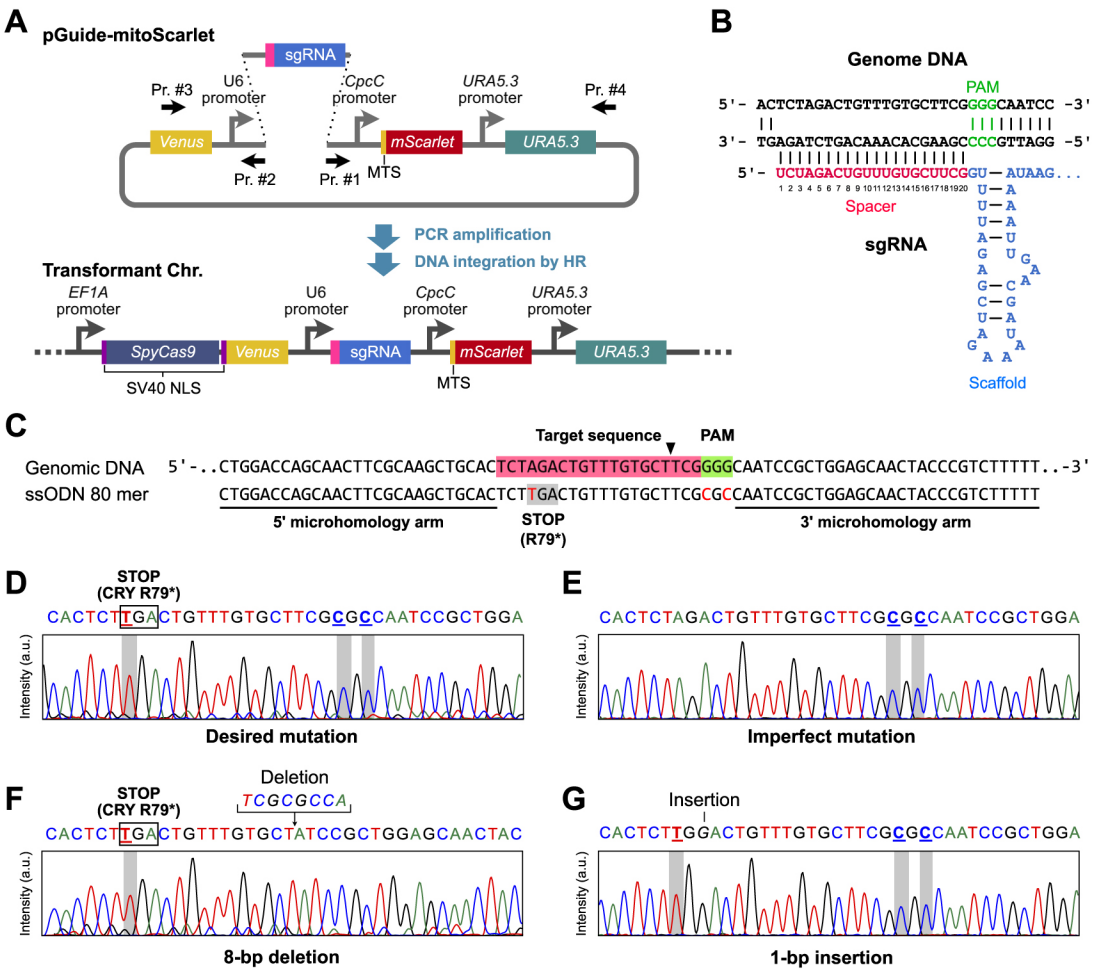

Fig. 2. Design and implementation of CRISPR-based genome editing in *Cyanidioschyzon merolae*. (A) Site-specific insertion of gene cassettes containing a sgRNA, a mitochondrion-targeted red fluorescent protein (mitoScarlet) and the selection marker *URA5.3*. A synthetic sgRNA is combined with a linearized plasmid amplified with primers #1 and #2 to generate pGuide-mitoScarlet. A PCR amplicon obtained with primers #3 and #4 is then inserted into the region downstream of *Cas9-Venus* in the YMT1 strain by homologous recombination. MTS, mitochondrial targeting signal. (B) Design of the sgRNA and the target site for the *CRY* locus. Base-pairing nucleotides (20 bp) are shown in magenta, the Cas9-binding hairpin in blue, and the protospacer-adjacent motif (PAM) sequence in green. (C) Principle of Cas9-mediated precise genome editing of the *CRY* locus. The arrowhead indicates the putative Cas9 cleavage site. An 80-nt single-stranded oligodeoxynucleotide (ssODN) donor template was designed to insert a stop codon and eliminate the PAM sequence in the *CRY* locus. The target sequence and the PAM are highlighted in magenta and green, respectively. The ssODN contains two 30-nt homology sequences (underlined). (D–G) Representative electropherograms from one experiment of mutated *CRY* across 13 independent edited colonies. (D) All targeted nucleotides in *CRY* were accurately edited in ten colonies. (E) Two of the three targeted nucleotides were edited in one colony. (F) An 8-bp deletion and (G) a 1-bp insertion were identified in one colony each.

genome editing and simultaneous visualization of the nucleus and mitochondrion in *C. merolae*; we named this CRISPR-based genome editing system CZON-cutter.

Phenotypic validation of the CRISPR-mediated *CRY* knockout strain by synchronization cultivation under distinct light conditions

To investigate whether *C. merolae CRY* affects cell cycle progression, we next tested the synchronization of CRISPR-generated *CRY* loss-of-function mutants (*cry*) under light–dark cycles using one strain as a representative. For this purpose, we selected the wild-type 10D strain rather than the uracil-auxotrophic YMT1 strain for control experiments to compare growth kinetics using culture conditions in non-uracil-supplemented medium. We cultured one *cry* strain and the wild-type 10D strain under light–dark cycles with white light (photon flux of 30 µmol m^{-2} s^{-1}). Given that about half (53.8% in this study) of the wild-type 10D cells are in the dividing phase 38 h after the initiation of synchronization, we compared the percentage of dividing cells in the knockout strain to that of the wild-type strain at this time point (Fig. 3B left; Table S1). Fewer cells appeared to be dividing in the *cry* strain (28.2%, $P<0.01$) relative to the wild-type strain, suggesting that inactivation of *CRY* may alter cell cycle progression, possibly by disrupting circadian rhythms in *C. merolae*.

Using the *cry* strain, we next explored the effect of light quality on entrainment of the circadian clock in *C. merolae*. We cultured *cry* and the wild-type strain under light–dark cycles consisting of a combination of blue and red light irradiation (Fig. 3B, middle; Table S1). To maintain photosynthetic activity, we adjusted the total photon flux to provide ∼30 µmol m^{-2} s^{-1} (blue, 15.4 µmol m^{-2} s^{-1}, red, 15.4 µmol m^{-2} s^{-1}). We observed that wild-type cells exhibit a comparable synchronization rate to that seen in white light, with a dividing rate of 53.6%. The percentage of dividing cells in the *cry* strain was significantly lower at 42.3% ($P<0.01$), although it was higher than that of the *cry* strain grown in white light.

Journal of Cell Science (2021) 134, jcs258948. doi:10.1242/jcs.258948

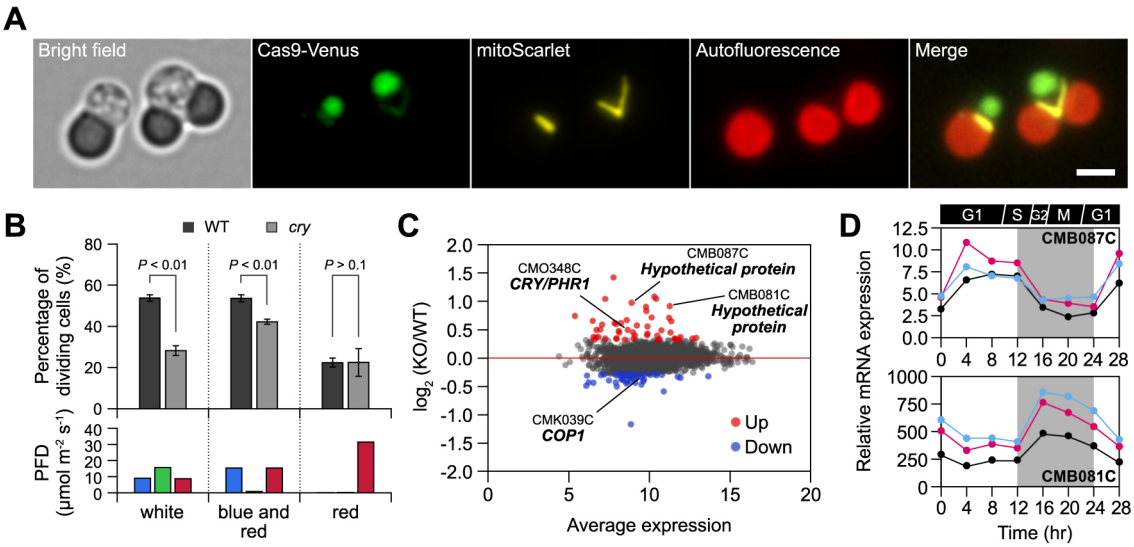

Fig. 3. CRY-dependent circadian clock entrainment by blue light stimuli in *Cyanidioschyzon merolae*. (A) Imaging of a non-dividing cell (left) and a dividing cell (right) in the *CRY* knockout (*cry*) strain. Green, Cas9-Venus fluorescence; yellow, mitoScarlet fluorescence; red, chlorophyll autofluorescence. Images are representative of more than five experiments. Scale bar: 2 µm. (B) Percentage of dividing cells in synchronized cultures for wild-type (WT) and *cry* strains under distinct light conditions. Total photon flux density (PFD) of blue, green, and red lights was kept at ∼30 µmol m^{-2} s^{-1} in each light condition. Data are represented as means±s.d. (*n*=3 from individual experiments). *P*-values are from a two-tailed unpaired Student's *t*-test. Raw data are given in Table S1. (C) MA plot of the fold-change [$\log_2$(KO/WT)] versus average expression of $\log_2$(TPM) from wild-type (WT) and *cry* (KO) samples. Expression values are given in Table S2. (D) Light-dependent expression changes of CMB087C and CMB081C. Black, WT strain; red, *CDKA* knockdown strain; blue, *RBR* knockout strain. Mean expression values in each strain were extracted from a time course (*n*=2) (Fujiwara et al., 2020).

As both the wild-type and the *cry* strains hardly proliferated under pure blue light, we could not confirm the synchronization properties of these strains under pure blue light conditions. Therefore, we also evaluated whether *C. merolae* cell division was entrained by blue light by culturing cells under pure red light (Fig. 3B, right; Table S1). Under these conditions, the percentages of dividing cells in the wild-type and *cry* strains were identical at 22.4% and 22.5%, respectively, indicating that the cell cycle of *C. merolae* is entrained by blue light irradiation. These findings suggest that *CRY* is involved in entrainment of the cell cycle by blue light in *C. merolae*. Although further experimental corroboration is required, these preliminary results suggest that *C. merolae* CRY may contribute to circadian entrainment, as the cell cycle is gated by the circadian clock (Yang et al., 2010).

Identification of putative components in the regulation mechanism of circadian rhythms in *C. merolae* by genome-wide transcriptome analysis using the *cry* strain

To explore the molecular links between cellular and organellar division and circadian rhythms in *C. merolae*, we compared gene expression profiles of the wild-type and the *cry* strains under continuous white light conditions by transcriptome deep sequencing (RNA-seq) (Fig. 3C). We identified the 50 most highly upregulated genes and the 50 most strongly downregulated genes between the two strains using a dataset from a single replicate (Table S2). *CRY* itself was among the upregulated genes in the *cry* strain, suggesting that an uncharacterized transcriptional activator may induce *CRY* expression to compensate for its loss. The expression level of the gene encoding the CRY regulatory protein, *CONSTITUTIVE PHOTOMORPHOGENIC1* (*COP1*), was lower in the *cry* strain. COP1 was originally identified as a key factor repressing light-mediated development and growth in plants by degrading photomorphogenic transcription factors in the dark (Lau and Deng, 2012). In addition, CRYs antagonize COP1 activity to regulate circadian rhythms in mammals (Rizzini et al., 2019). As the loss of CRY function affected cell synchronization and the expression levels of *COP1*, *C. merolae* CRY may also play a pivotal role in the regulation of circadian rhythms in this alga.

RNA-seq analysis indicated that 40% of the differentially expressed genes have unknown biological functions in the *C. merolae* genome database, hinting that some of these genes might act as nodes linking the circadian clock with the cellular and organellar division cycle. We independently validated the expression pattern of two of the most highly upregulated genes in our dataset, CMB087C and CMB081C, over a diurnal time course, with a peak in expression in the middle of the light period (CMB087C) or dark period (CMB081C), respectively (Fig. 3D). This diurnal pattern remained unchanged in knockout strains of either the *CYCLIN-DEPENDENT KINASE A* (*CDKA*) or the *RETINOBLASTOMA-RELATED* (*RBR*) genes. Thus, further exploration of the function of these genes may reveal the regulatory system underlying cellular/organellar division and circadian rhythms.

Gene cassette knock-in for knocking out a target gene and fluorescent protein labeling of the peroxisome by CZON-cutter

We next used CZON-cutter to insert a sequence of interest into the genome (knock-in) while also knocking out a target gene and marking the single peroxisome with another fluorescent protein. We selected *ACTIN* as a target for gene knock-in. Although the *C. merolae* genome contains a single *ACTIN* gene (Matsuzaki et al., 2004; Takahashi et al., 1995), cytokinesis in *C. merolae* does not involve actin (Yagisawa et al., 2020). As actin plays a central role in cell division in contemporary eukaryotes, direct evidence of actin-free cell division in *C. merolae* would illustrate a new framework for cytokinesis in simpler eukaryotes. To generate a construct for CRISPR-mediated gene knock-in, we modified the sgRNA cloned into the pGuide-mitoScarlet plasmid to target

Journal of Cell Science (2021) 134, jcs258948. doi:10.1242/jcs.258948

ACTIN. We also constructed a plasmid that would act as template for HDR, pCer3-PTS1, in which the constitutive *ApcC* promoter derived from the 5′ UTR of *ApcC* encoding allophycocyanin-associated rod linker protein drives the expression of the gene encoding cyan fluorescence protein mCerulean3 fused to a peroxisome targeting signal (mCerulean3-PTS1, hereafter perCerulean3), followed by the *TUBB* 3′ UTR (Fig. 4A). Target site specificity was provided by the PCR primers, which included 50-nt overhangs with homology to the target locus of interest (Fig. 4B,C). We transformed the YMT1 strain with a pool of these two PCR products (one derived from pGuide-mitoScarlet-ACTIN and one from pCer3-PTS1) and obtained three uracil-autotrophic colonies expressing both *mitoScarlet* and *perCerulean3* (~2.6 transformants per 10^8 cells).

We chose one *ACTIN* knockout (*actin*) strain as a representative for further analysis and confirmed the presence of *perCerulean3* at the *ACTIN* locus (Fig. 4D; Fig. S2). We then used fluorescence microscopy to image the peroxisome, nucleus, mitochondrion and chloroplast in the same cell. We noticed no significant differences in the growth curves or cell shapes of the wild-type and *actin* strains over the cell cycle (Fig. 4E,F), and observations via fluorescence microscopy demonstrated that cells lacking actin undergo cytokinesis successfully and divide into two daughter cells, each with its own nucleus, mitochondrion, chloroplast, and peroxisome (Fig. 4G). We conclude that actin is not required for cell growth or proliferation in *C. merolae*. In addition, we confirmed that the *perCerulean3* cassette can be inserted into the *CRY* locus using the same approach, resulting in transformants that accumulate the fluorescent reporters as seen in the *actin* strain (Fig. S3), suggesting that the CZON-cutter platform can insert the *perCerulean3* cassette with 50-nt short homology arms into any locus of interest.

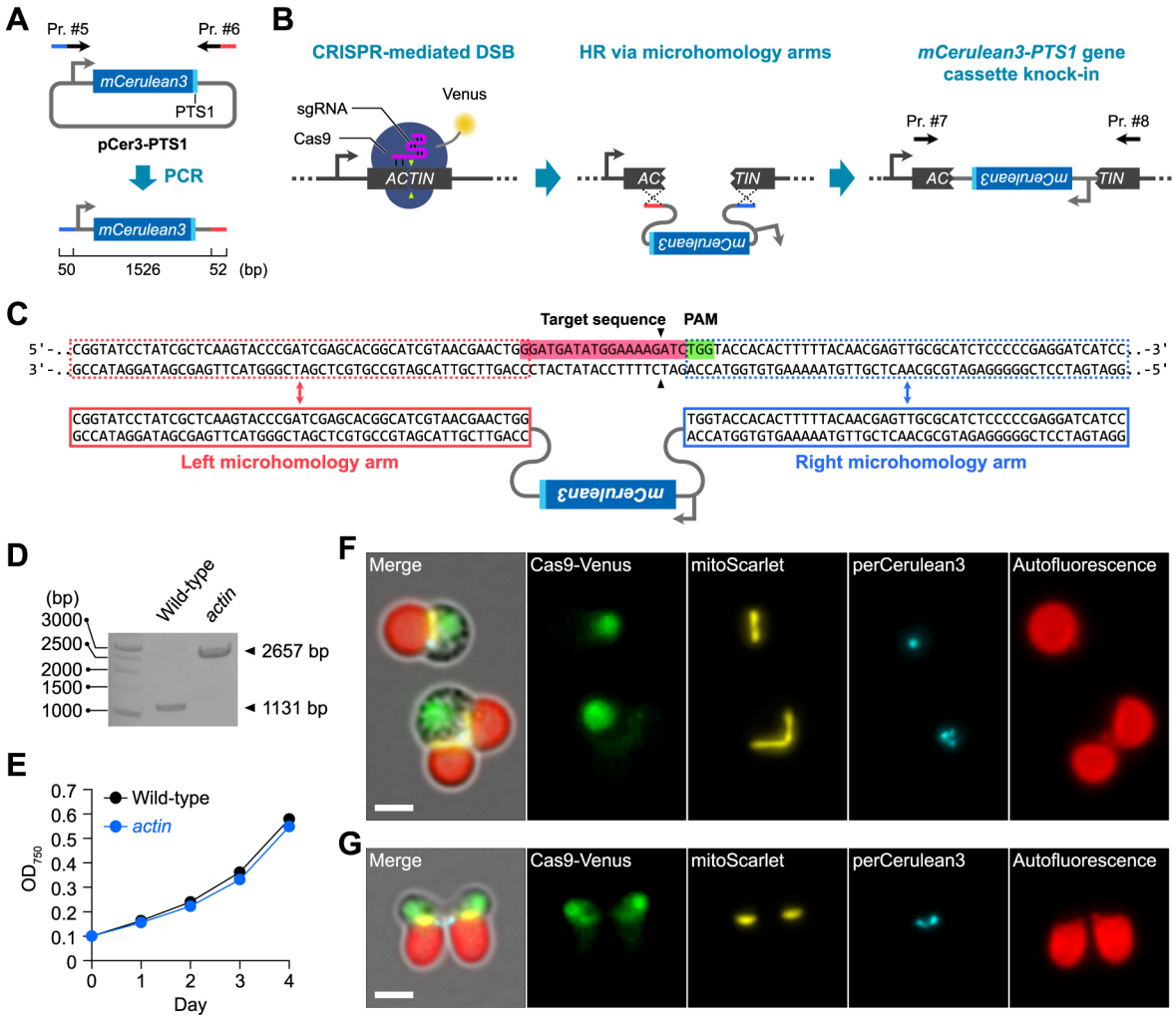

Fig. 4. Site-specific knock-in of a cassette encoding mCerulean3 fused to a peroxisomal targeting signal by CZON-cutter. (A) PCR amplification of a gene cassette encoding mCerulean3 with a peroxisomal targeting signal. The double-stranded DNA fragment containing the *ApcC* promoter, the *mCerulean3* coding sequence with a peroxisomal targeting signal (PTS1), and the *TUBB* 3′ UTR and ~50-bp microhomology arms on either side (total length: 1626 bp) were amplified by PCR using primers #5 and #6. (B) Principle behind knocking in a fluorescent reporter expression cassette at the *ACTIN* locus. (C) Principle of Cas9-mediated gene cassette knock-in at the *ACTIN* locus. The arrowheads indicate the putative Cas9 cleavage site. The target sequence and the PAM are highlighted in magenta and green, respectively. Flanking microhomology sequences of the *perCerulean3* cassette are shown in red and blue boxes. (D) Confirmation of the knock-in event at the *ACTIN* locus by PCR with primers #7 and #8 shown in B. The wild-type strain was used as a negative control. Image is representative of three experiments. (E) Growth curves of the wild-type strain and the *ACTIN* knockout (*actin*) strain. Data are shown as means (n=3 from cell culture replicates). (F) Representative images of a non-dividing cell (top) and a dividing cell (bottom) of the *actin* strain. Green, Cas9-Venus fluorescence; yellow, mitoScarlet fluorescence; blue, perCerulean3 fluorescence; red, chlorophyll autofluorescence. (G) Representative image of a single cell from the *actin* strain at the cytokinetic abscission stage. Images in F and G are representative of more than five experiments. Scale bars: 2 µm.

Journal of Cell Science (2021) 134, jcs258948. doi:10.1242/jcs.258948

Monitoring living transformants to evaluate the effect of knocking out essential genes

Next, we assessed the applicability of the CZON-cutter platform to test the potential contribution of a given gene during organellar and cellular division, even when the gene is essential for growth and/or proliferation. For this purpose, we modified the sgRNA in the pGuide-mitoScarlet plasmid to target *MDR1* or *TUBG* (encoding γ-Tubulin). MDR1 participates in the assembly of the mitochondrion-dividing (MD) ring, the molecular machinery that severs the mitochondrion for mitochondrial proliferation (Yoshida et al., 2017), whereas γ-Tubulin plays a critical role in spindle assembly and chromosome segregation during M phase (Wiese and Zheng, 2006). We predicted that inactivation of MDR1 or γ-Tubulin would result in severe, abnormal mitochondrial division and cell division phenotypes.

To evaluate the effect of knocking out these genes, we first investigated the morphology of transformants 2 days after transformation with PCR amplicons for the sgRNA targeting *MDR1* and the *perCerulean3* fluorescence reporter. We identified cells with fluorescence from mScarlet in the mitochondrion and mCerulean3 in the peroxisome, which comprised ∼0.1% of all cells, indicative of our transformation efficiency (Fig. 5A). Since we detected fluorescence from both reporters (mitoScarlet for sgRNA and perCerulean3 for gene knock-in) by fluorescence microscopy, we hypothesized that the *perCerulean3* cassette is integrated at the *MDR1* locus, thereby knocking it out.

A morphological examination of transformants showed an obstruction of mitochondrial division and mitochondrion overgrowth. Furthermore, we also noticed nuclear division defects, peroxisomal division defects, and an enlargement of cells. The

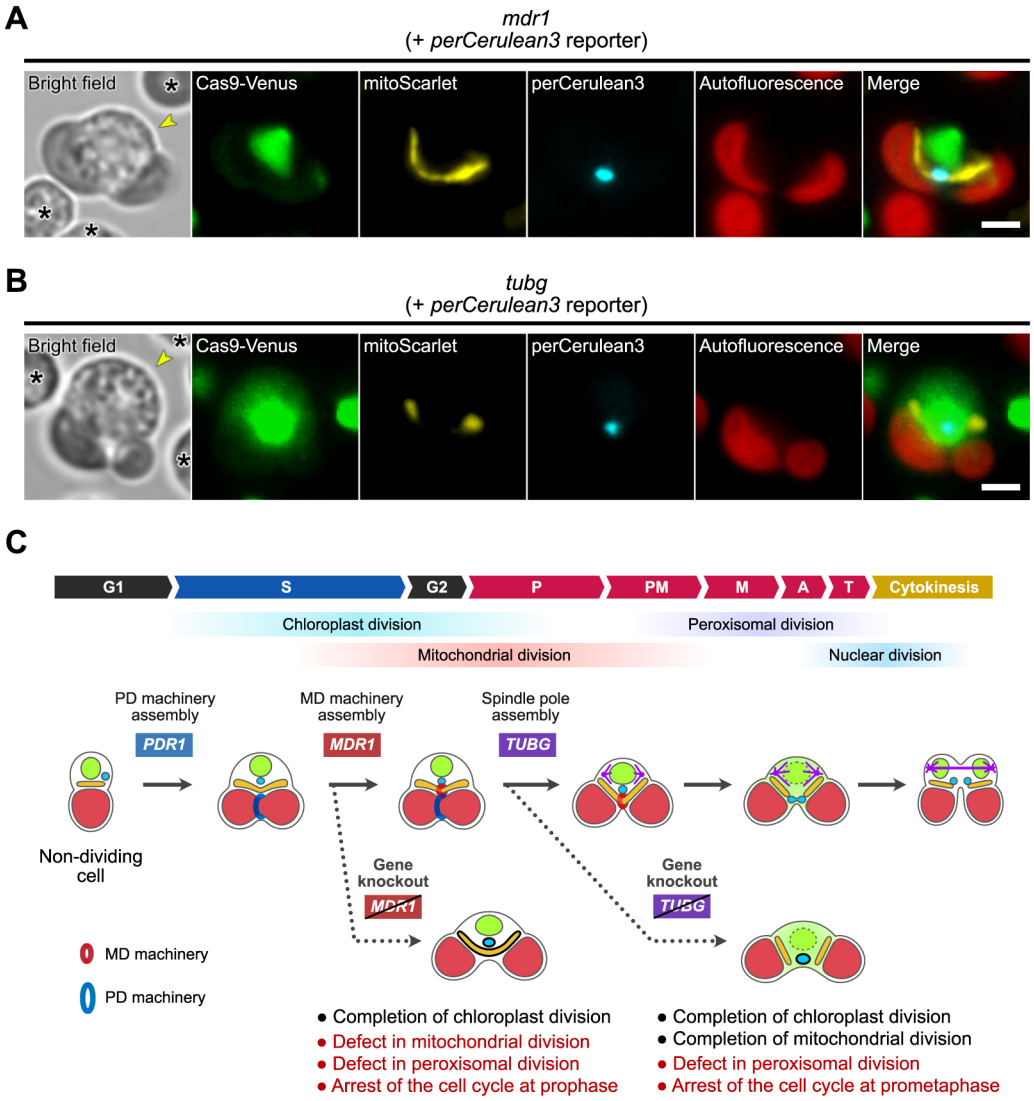

Fig. 5. Essential genes for organellar and cellular division can be targeted by CZON-cutter. (A,B) Representative images of a *MDR1* knockout (*mdr1*) cell and a *TUBG* knockout (*tubg*) cell. The cells were imaged 2 days after transformation. As these are living cells, they floated in the mounting medium and shifted slightly during imaging; the transformed cell (yellow arrowhead) is shown in the center of the field, while non-transformed cells are indicated with asterisks. Each gene was knocked out by inserting the *perCerulean3* cassette at the target locus. Images in A and B are representative of more than five experiments. Scale bars: 2 µm. (C) Schematic illustrations of morphological phenotypes of wild-type, *mdr1* and *tubg* cells via CZON-cutter. When a target gene does not affect organellar and/or cellular division, transformed cells undergo normal organellar divisions and cytokinesis, as shown here. However, when a target gene is involved in division, such as *MDR1* or *TUBG*, the resulting transformed cells become arrested at a particular cell division phase with abnormal morphology specific for each organellar division defect.

Journal of Cell Science (2021) 134, jcs258948. doi:10.1242/jcs.258948

fluorescence derived from Cas9-Venus allowed us to identify the nucleus in each cell; together with the presence of an overgrown mitochondrion, these observations suggested that the nuclear envelope is intact and that the transformant is arrested in prophase. The observed phenotype of mitochondrial division defects is very similar to that previously reported for antisense suppression of *MDR1* (Yoshida et al., 2017), suggesting that the gene knockout approach employing CZON-cutter will be an effective method for studying genes related to organellar and cellular division.

Finally, we knocked out *TUBG* and characterized the resulting phenotypes with the same strategy. Two days after transformation, we identified cells exhibiting mitoScarlet and perCerulean3 fluorescence at a similar frequency (~0.1%) as with *MDR1* (Fig. 5B). Although we detected strong fluorescence for Cas9-Venus in the putative nuclear region, we also observed some fluorescence in the cytosol, indicating that the nuclear envelope is partially disassembled and that the transformant is arrested in prometaphase or metaphase. In addition, the chloroplast and mitochondrion had already undergone division, while we observed a single peroxisome in one of the two dividing cells. The results indicate that the division of each organelle – chloroplast, mitochondrion, and peroxisome – occurs at different times during the cell cycle (Fig. 5C). The CZON-cutter platform will be instrumental in exploring the function of genes involved in organellar and cellular division, even if the gene is essential.

DISCUSSION

CRISPR-mediated genome editing with multiplexed organelle visualization in *C. merolae*

The unique cell structure and availability of the complete genome sequence of *C. merolae* offers a new avenue to study intracellular mechanisms of eukaryotic cells. Here, we describe an efficient and accurate gene-targeting method to take advantage of the unique features of this unicellular alga. Conventional HR techniques in *C. merolae* involve the introduction of a linear DNA fragment consisting of a gene cassette and selection marker flanked by over 1 kb of sequence from the locus of interest on either side (Fujiwara et al., 2017). The generation of a transformation construct therefore entails multiple steps, and the resulting plasmid is rather large and complex (Fig. 1A). Although *C. merolae* boasts the smallest genome of all photosynthetic eukaryotes, cumbersome gene targeting has hindered genome-wide analyses of gene function in this alga. Here, we established the CRISPR-mediated genome-editing platform CZON-cutter, which can disrupt or modify any gene in the genome with the added benefit of multiplexed visualization of organelles in a simple procedure (Fig. 1B; Figs S4 and S5). The engineered strain used here, YMT1, showed no abnormal growth phenotype (Fig. 1E). Given the small size of the *C. merolae* genome, potential off-target effects by CZON-cutter should be minimal. Furthermore, multiplexed visualization of organelles with bright fluorescence proteins allows the prompt characterization of the phenotypes associated with a gene knockout in terms of organellar division and morphology.

The CZON-cutter platform provides an efficient, versatile and high-throughput approach to investigate the biological function of any gene at organellar resolution

Mitochondria and chloroplasts proliferate via binary division of preexisting organelles by using specialized ring-shaped complexes called mitochondrial- and plastid-division machineries (Yoshida and Mogi, 2019; Yoshida et al., 2010, 2017). Peroxisomes divide by using a homologous division machinery (Imoto et al., 2013). However, the individual components and the underlying regulatory mechanisms of these division machineries are largely unknown. A recent transcriptome study identified 181 uncharacterized genes that are specifically expressed during mitochondrial and chloroplast division (Fujiwara et al., 2020), which may be candidate genes for exploring the mechanisms behind organellar division.

In this study, we generated a knockout strain for *CRY* with CZON-cutter, which revealed that CRY may be a blue light photoreceptor with critical roles in the regulation of cell cycle progression in *C. merolae*. CZON-cutter also paves the way for studies of the physiological and molecular mechanisms of the cell cycle. Furthermore, the successful knockout of *MDR1* and *TUBG* also demonstrated that CZON-cutter makes it possible to evaluate the function of essential genes (Fig. 5). In addition, our results hint at the links between organellar division and cellular division. A defect in mitochondrial division caused by genome editing of *MDR1* arrested cell cycle progression at prophase, indicating that mitochondrial division may participate in a prophase–prometaphase checkpoint. Another notable illustration of the power of CZON-cutter is evident in the gene knockout of *TUBG*, which not only blocked chromosome segregation but also caused a peroxisomal division defect. These results indicate that chloroplast, mitochondrial and peroxisomal divisions are executed in a specific sequence during the cell cycle and that completion of each organellar division is likely to serve as a checkpoint in the cell cycle. Further studies will aim to explore the molecular mechanisms of this highly interdependent system between division of organelles and the cell. In conclusion, CZON-cutter enables the systematic analysis of gene function by genome editing and multiplexed organellar visualization. The originality and versatility of CZON-cutter will help accelerate gene discovery to reveal biological principles of the cell.

MATERIALS AND METHODS

C. merolae YMT1 strain

To create a *C. merolae* strain constitutively accumulating nuclear-localized Cas9 fused to Venus, a construct containing *Cas9-Venus* and chloroplast-targeted *CAT* was assembled as follows. The *EF1A* promoter (1 kb) was PCR amplified using genomic DNA from *C. merolae* strain 10D as template. A version of *S. pyogenes Cas9*, codon-optimized for mammalian expression and fused to the sequence of three copies of the FLAG tag and two copies of a nuclear localization signal from simian virus 40 (SV40), was PCR-amplified from plasmid pKIR1.1 (Addgene #85758). *Venus* codon-optimized for expression in *C. merolae* (Nagai et al., 2002) and fused to the sequence of three copies of the HA tag, the *UBQ3* (*UBIQUITIN 3*) 3′ UTR, the *ApcC* promoter and *CAT* fused to a chloroplast transit peptide (CTP) derived from ApcC, and the *TUBB* (*β-Tubulin*) 3′ UTR were amplified by PCR using plasmid pVenus-CAT (gift from Takayuki Fujiwara, National Institute of Genetics, Japan) as template. The resulting PCR amplicons were cloned into a linear vector amplified by PCR using p*NIR*p::sfGFP (gift from T. Fujiwara) (Fujiwara et al., 2015) as template. The resulting construct, pCas9-Venus-CAT, contained the gene cassettes *Cas9-Venus* and *CTP-CAT* ~0.9 kb upstream of *URA5.3*. For the construction of pCas9-Venus-CAT, PCR amplification and assembly of DNA fragments were performed with Platinum SuperFi II DNA polymerase (Thermo Fisher Scientific) and the NEBuilder HiFi DNA assembly cloning kit (New England Biolabs), respectively. Finally, using pCas9-Venus-CAT as template, a PCR amplicon was amplified that contained ~1400 bp of sequence upstream of *URA5.3* (from −2300 to −898 bp), the *EF1A* promoter, *Cas9-Venus*, the *UBQ3* 3′ UTR, the *ApcC* promoter, *CTP-CAT*, the *TUBB* 3′ UTR and ~900 bp of sequence upstream of *URA5.3* (−897 to −1 bp). The PCR amplicon was introduced into the uracil-auxotrophic mutant M4 cells by polyethylene glycol (PEG)–mediated transformation as described by Ohnuma et al. (2008), Imamura et al. (2009) and Fujiwara et al. (2015). Chloramphenicol-resistant transformants were selected by cultivation on chloramphenicol-containing medium at 150 µg ml^{-1} for 15 days as described by Fujiwara et al. (2017). After chloramphenicol selection, transformants were spread on modified Allen's (MA) medium supplemented with uracil (0.5 mg ml^{-1}) to isolate single

colonies. Accumulation of Cas9-Venus was examined by fluorescence microscopy, and the presence of the introduced DNA was confirmed by direct colony PCR and sequencing. The full amino acid sequence of Cas9-Venus is given in Table S5.

Construction of sgRNA expression vectors

To generate the sgRNA expression vector (pGuide-mitoScarlet), the *C. merolae* U6 promoter and a sgRNA scaffold with a termination signal were synthesized. The synthetic DNA fragments were assembled with a linear vector DNA containing 2300 bp of *URA5.3* upstream sequence and the *URA5.3* open reading frame, PCR amplified using p*NIR*p::sfGFP (Fujiwara et al., 2015) as a template. Then, the *UBQ3* 3′ UTR, the *CpcC* promoter, the MTS derived from mitochondrial *EF-Tu*, *mScarlet* (Bindels et al., 2016) codon-optimized for *C. merolae* expression and the *TUBB* 3′ UTR were introduced into the vector. Finally, the *URA5.3* upstream sequence (from −2300 to −898 bp) was replaced by *Venus* and the *UBQ3* 3′ UTR to create a HR site to introduce constructs into the YMT1 strain. Two types of procedures for construction of the pGuide-mitoScarlet plasmid targeting a target locus are shown in Fig. S4. Potential Cas9 target sites in the *CRY*, *ACTIN*, *MDR1* and *TUBG* loci were searched using the CRISPRdirect web server (http://crispr.dbcls.jp/) using the genome of *C. merolae* ASM9120v1 (Table S3). To create the sgRNA expression vector targeting *CRY* (pGuide-$CRY_{232\text{-}254}$-mitoScarlet), a 497-bp synthesized DNA fragment containing a sgRNA spacer sequence targeting nucleotides 232–254 of the *CRY* locus was assembled with a linear vector amplified by PCR with primer sets #1 and #2 using pGuide-mitoScarlet as the template. Similarly, the sgRNA expression vectors targeting *ACTIN* (pGuide-$ACTIN_{239\text{-}261}$-mitoScarlet) and *MDR1* (pGuide-$MDR1_{254\text{-}276}$-mitoScarlet) were constructed from synthesized DNA fragments containing a sgRNA spacer sequence targeting the *ACTIN* or *MDR1* locus, respectively. The complete nucleotide sequences of synthetic DNAs for sgRNAs targeting the *CRY*, *ACTIN*, and *MDR1* loci are given in Table S4 as #16 to #18. To create the sgRNA expression vector targeting *TUBG* (pGuide-$TUBG_{863\text{-}885}$-mitoScarlet), a 62-bp ssODN (#9) containing a sgRNA spacer sequence targeting nucleotides 863–885 bp of the *TUBG* locus was assembled with a linear vector amplified by PCR with primer sets #10 and #11 using pGuide-mitoScarlet as template. One guanine nucleobase was added at the 5′ side of the target sequence for *CRY* and *TUBG* to stimulate transcription of sgRNA *in vivo*.

The plasmid containing peroxisome-targeted *mCerulean3* codon-optimized for *C. merolae* expression was constructed as follows. A synthesized DNA fragment containing *mCerulean3* was cloned into a vector pUC57. *mCerulean3* (Markwardt et al., 2011) fused to peroxisomal targeting signal 1 (PTS1) was amplified by PCR with primer sets #19 and #20 using the above plasmid as template to generate peroxisome-targeted *mCerulean3* (*perCerulean3*). The *ApcC* promoter, *perCerulean3*, the *TUBB* 3′ UTR and the pUC57 vector were amplified by PCR using primer sets #19 to #26 and assembled into a new vector named pCer3-PTS1. The full nucleotide sequence of *perCerulean3* is given in Table S6.

For all plasmids, PCR amplification and assembly of DNA fragments were performed using Platinum SuperFi II DNA polymerase (Thermo Fisher Scientific) and the NEBuilder HiFi DNA assembly cloning kit (New England Biolabs), respectively. Primer sequences are given in Table S4.

Genome editing experiments

For genome editing of the *CRY* locus, a PCR amplicon was amplified from pGuide-$CRY_{232\text{-}254}$-mitoScarlet as template and contained the sgRNA targeting nucleotides 232–254 of the *CRY* locus, mitochondrion-targeted red fluorescent protein mScarlet (*mitoScarlet*) and the selection marker *URA5.3*, flanked by HR sites. The PCR amplicon was then mixed with an 80-nt ssODN (Fig. 2C) consisting of a 20-nt target sequence and two 30-nt flanking upstream and downstream sequences of the target sequence. The mixture was then transformed into YMT1 cells as described by Fujiwara et al. (2015). For gene knock-in at the target locus, PCR amplicons were amplified with primer sets #3 and #4 from pGuide-$ACTIN_{239\text{-}261}$-mitoScarlet, pGuide-$MDR1_{254\text{-}276}$-mitoScarlet, or pGuide-$TUBG_{863\text{-}885}$-mitoScarlet as templates; each PCR product consisted of the respective sgRNA, *mitoScarlet* and *URA5.3* flanked with HR sites. In addition, the *perCerulean3* cassette was PCR amplified with short homology arms with primer sets #5 and #6 (for *ACTIN*), #27 and #28 (for *CRY*), #12 and #13 (for *MDR1*), or #14 and #15 (for *TUBG*) using pCer3-PTS1 as template. The resulting PCR amplicons (from pGuide-mitoScarlet and pCer3-PTS1) were then mixed and introduced into YMT1 cells as described by Fujiwara et al. (2015).

Fluorescence microscopy

Fluorescence observations were conducted on an Olympus IX83 inverted microscope with a 1.45 NA, 100× oil immersion objective. Illumination was provided by a fluorescent light source (U-HGLGPS; Olympus), and the samples were observed through excitation filters [490-500HQ (Olympus) for Venus, FF01-549/12-25 (Semrock) for mScarlet, FF01-427/10-25 (Semrock) for mCerulean3, and FF01-405/10-25 (Semrock) for chloroplasts], custom dichroic mirrors [Di03-R514-t1-25×36 (Semrock) for Venus, Di03-R561-t1-25×36 (Semrock) for mScarlet, FF458-Di02-25×36 (Semrock) for mCerulean3, and T455lp (Chroma) for chloroplasts], and emission filters [FF02-531/22-25 (Semrock) for Venus, FF02-585/29-25 for mScarlet (Semrock), FF01-474/27-25 for mCerulean3, and FF02-617/73-25 for chloroplasts (Semrock)]. Images were acquired with a Zyla 4.2 sCMOS camera (Andor) controlled by MetaMorph software (Molecular Devices). The effective pixel size was 65.2 nm×65.2 nm.

Cell cultures and synchronization cultivation

C. merolae 10D strain cells (NIES-3377) were used as the wild type in this study. Wild-type cells and CRISPR-generated mutants were maintained on 2× Allen's medium (Allen, 1959). The uracil-auxotrophic M4 strain and the uracil-auxotrophic/chloramphenicol-resistant YMT1 strain were maintained on MA2 medium (Ohnuma et al., 2008) supplemented with uracil (0.5 mg ml^{-1}) and 5-fluoroorotic acid monohydrate (0.8 mg ml^{-1}). All strains were cultured in flasks with agitation at 120 rpm under continuous white light (22 µmol m^{-2} s^{-1}) at 38°C.

For synchronization of cultivation, cells were subcultured to <10^7 cells ml^{-1} in a 100-ml flask and bubbled with filtered clean and humidified air through a tube connected to an aquarium pump. Cells were then incubated under a 12-h-light–12-h-dark cycle at 42°C in a SLI-700 incubator (EYELA). Blue and red light irradiation were supplied using 470 nm ±20 nm LEDs (ISL-150×150-HBB; CCS Inc.) and 660 nm±20 nm LEDs (ISL-150×150-RR; CCS Inc.), respectively.

Phylogenetic analysis

The GenBank accession numbers used were as follows: *Cyanidioschyzon merolae* CRY/PHR1 (XP_005537706), *C. merolae* PHR2 (BAM80259), *C. merolae* PHR3 (BAM80957), *C. merolae* PHR4 (BAM79915), *C. merolae* PHR5 (BAM78760), *C. merolae* PHR7 (BAM82280), *Arabidopsis thaliana CRY1* (AEE82696), *A. thaliana CRY2* (AEE27692), *A. thaliana CRY-DASH* (Q84KJ5), *Homo sapiens CRY1* (NP_004066), *H. sapiens CRY2* (Q49AN0), *Mus musculus CRY1* (AAD39548), *M. musculus CRY2* (AAD46561), *Gallus gallus* CRY1 (AAK61385), *G. gallus* CRY2 (AAK61386), *G. gallus* CRY4 (NP_001034685), *Drosophila melanogaster* CRY (NP_732407), *D. melanogaster* 6-4 photolyase (BAA12067), *Escherichia coli* DNA photolyase (WP_062883603), and *Synechocystis* sp. PCC 6803 DNA photolyase (Q55081).

The phylogenic tree was generated with MEGA X (Kumar et al., 2018). Amino acid sequences were aligned with the ClustalW algorithm with default settings in MEGA X using the maximum likelihood method with the LG+G+I model. The local probability of each branch was calculated using the neighbor-joining method with 1000 replications.

RNA sequencing and analysis

Cells for the wild-type (10D) strain and a single *cry* strain were grown in 2× Allen's medium under continuous white light for 3 days at 40°C and harvested from a 15-ml culture [optical density at 750 nm (OD_{750}) of 0.6] by centrifugation at 1500 ***g*** for 5 min at room temperature. Total RNA was purified using the Trizol/RNeasy hybrid protocol (Trizol, Life Technologies; RNeasy Mini Kit, Qiagen). Polyadenylated [poly(A)] RNA was then purified with the NEBNext Poly(A) mRNA Magnetic Isolation

Module (NEB, E7490). Sequencing libraries were constructed with the NEBNext Ultra II Directional RNA Library Prep kit for Illumina (NEB, E7760), amplified with custom oligonucleotides, and sequenced as 150-bp paired-end reads on an Illumina NovaSeq sequencer at GENEWIZ Inc. After adaptor trimming and removing low-quality reads by Trimmomatic-0.39 (Bolger et al., 2014), clean reads were mapped to the *C. merolae* genome (ASM9120v1) using bowtie2 and counted by featureCounts (Langmead and Salzberg, 2012; Liao et al., 2014). The RNA-seq experiment was performed using a single replicate. Genes with over 100 reads were selected and their expression normalized to transcripts per kilobase million (TPM). We identified the top upregulated and downregulated genes between the wild-type and the *cry* strains from the Log_2 (fold-change) of TPM-normalized read counts. The genes are listed in Table S2.

Acknowledgements
We thank our lab colleagues for their support and advice during this project.

Competing interests
The authors declare no competing or financial interests.

Author contributions
Conceptualization: Y.Y.; Methodology: Y.M., T.F., Y.Y.; Validation: N.T., Y.M., K.Y., Y.T., T.H., Y.Y.; Formal analysis: N.T., Y.M., K.Y., Y.T., Y.Y.; Investigation: N.T., Y.M., T.F., Y.Y.; Resources: Y.M., T.F.; Data curation: N.T., Y.M., Y.Y.; Writing - original draft: N.T., Y.M., T.H., Y.Y.; Visualization: N.T., Y.M., Y.Y.; Supervision: Y.Y.; Project administration: Y.Y.; Funding acquisition: T.F., T.H., Y.Y.

Funding
This work was supported by PRESTO from the Japan Science and Technology Agency (JPMJPR20EE to Y.Y.); the Human Frontier Science Program Career Development Award (no. CDA00049/2018-C to Y.Y.); Japan Society for the Promotion of Science KAKENHI (no. JP18K06325 to Y.Y. and 18K06300 to T.F.); the Sumitomo Foundation (no. 180705 to Y.Y.); the Institute for Fermentation, Osaka (L-2020-2-008 to Y.Y.); the Grant-in-Aid for Scientific Research on Innovative Areas from the Ministry of Education, Culture, Sports, Science, and Technology of Japan (no. 16H06465 to T.H. and Y.Y.); and CREST from the Japan Science and Technology Agency (JPMJCR20E5 to T.H.).

Data availability
Raw RNA sequencing data have been deposited into the Sequence Read Archive (SRA) with project ID PRJNA773182.

References
Adli, M. (2018). The CRISPR tool kit for genome editing and beyond. *Nat. Commun.* **9**, 1911. doi:10.1038/s41467-018-04252-2

Allen, M.B. (1959). Studies with Cyanidium caldarium, an anomalously pigmented chlorophyte. *Arch. Mikrobiol.* **32**, 270-277. doi:10.1007/BF00409348

Asimgil, H. and Kavakli, I. H. (2012). Purification and characterization of five members of photolyase/cryptochrome family from *Cyanidioschyzon merolae*. *Plant Sci.* **185–186**, 190-198. doi:10.1016/j.plantsci.2011.10.005

Bindels, D. S., Haarbosch, L., Van Weeren, L., Postma, M., Wiese, K. E., Mastop, M., Aumonier, S., Gotthard, G., Royant, A., Hink, M. A. et al. (2016). mScarlet: a bright monomeric red fluorescent protein for cellular imaging. *Nat. Methods* **14**, 53-56. doi:10.1038/nmeth.4074

Bolger, A. M., Lohse, M. and Usadel, B. (2014). Trimmomatic: a flexible trimmer for Illumina sequence data. *Bioinformatics* **30**, 2114-2120. doi:10.1093/bioinformatics/btu170

Chaves, I., Pokorny, R., Byrdin, M., Hoang, N., Ritz, T., Brettel, K., Essen, L. O., van der Horst, G. T. J., Batschauer, A. and Ahmad, M. (2011). The cryptochromes: Blue light photoreceptors in plants and animals. *Annu. Rev. Plant Biol.* **62**, 335-364. doi:10.1146/annurev-arplant-042110-103759

Fell, V. L. and Schild-Poulter, C. (2015). The Ku heterodimer: function in DNA repair and beyond. *Mutat. Res. Rev. Mutat. Res.* **763**, 15-29. doi:10.1016/j.mrrev.2014.06.002

Fujiwara, T., Tanaka, K., Kuroiwa, T. and Hirano, T. (2013). Spatiotemporal dynamics of condensins I and II: Evolutionary insights from the primitive red alga *Cyanidioschyzon merolae*. *Mol. Biol. Cell* **24**, 2515-2527. doi:10.1091/mbc.e13-04-0208

Fujiwara, T., Kanesaki, Y., Hirooka, S., Era, A., Sumiya, N., Yoshikawa, H., Tanaka, K. and Miyagishima, S. Y. (2015). A nitrogen source-dependent inducible and repressible gene expression system in the red alga *Cyanidioschyzon merolae*. *Front. Plant Sci.* **6**, 1-10. doi:10.3389/fpls.2015.00657

Fujiwara, T., Ohnuma, M., Kuroiwa, T., Ohbayashi, R., Hirooka, S. and Miyagishima, S. Y. (2017). Development of a double nuclear gene-targeting method by two-step transformation based on a newly established chloramphenicol-selection system in the red alga *Cyanidioschyzon merolae*. *Front. Plant Sci.* **8**, 1-10. doi:10.3389/fpls.2017.00343

Fujiwara, T., Hirooka, S., Ohbayashi, R., Onuma, R. and Miyagishima, S.-Y. (2020). Relationship between cell cycle and diel transcriptomic changes in metabolism in a unicellular red alga. *Plant Physiol.* **183**, 1484-1501. doi:10.1104/pp.20.00469

Gillham, N. W., Boynton, J. E. and Hauser, C. R. (1994). Translational regulation of gene expression in chloroplasts and mitochondria. *Annu. Rev. Genet.* **28**, 71-93. doi:10.1146/annurev.ge.28.120194.000443

Gray, M. W. W. (1992). The endosymbiont hypothesis revisited. *Int. Rev. Cytol.* **141**, 233-357. doi:10.1016/S0074-7696(08)62068-9

Imamura, S., Kanesaki, Y., Ohnuma, M., Inouye, T., Sekine, Y., Fujiwara, T., Kuroiwa, T. and Tanaka, K. (2009). R2R3-type MYB transcription factor, CmMYB1, is a central nitrogen assimilation regulator in Cyanidioschyzon merolae. *Proc. Natl. Acad. Sci.* **106**, 14180-14180. doi:10.1073/pnas.0902790106

Imoto, Y., Fujiwara, T., Yoshida, Y., Kuroiwa, H., Maruyama, S. and Kuroiwa, T. (2010). Division of cell nuclei, mitochondria, plastids, and microbodies mediated by mitotic spindle poles in the primitive red alga *Cyanidioschyzon merolae*. *Protoplasma* **241**, 63-74. doi:10.1007/s00709-010-0107-y

Imoto, Y., Kuroiwa, H., Yoshida, Y., Ohnuma, M., Fujiwara, T., Yoshida, M., Nishida, K., Yagisawa, F., Hirooka, S., Miyagishima, S. Y. et al. (2013). Single-membrane-bounded peroxisome division revealed by isolation of dynamin-based machinery. *Proc. Natl. Acad. Sci. U.S.A.* **110**, 9583-9588. doi:10.1073/pnas.1303483110

Jiang, F. and Doudna, J. A. (2017). CRISPR–Cas9 structures and mechanisms. *Annu. Rev. Biophys.* **46**, 505-529. doi:10.1146/annurev-biophys-062215-010822

Kobayashi, Y., Imamura, S., Hanaoka, M. and Tanaka, K. (2011). A tetrapyrrole-regulated ubiquitin ligase controls algal nuclear DNA replication. *Nat. Cell Biol.* **13**, 483-487. doi:10.1038/ncb2203

Kumar, S., Stecher, G., Li, M., Knyaz, C. and Tamura, K. (2018). MEGA X: Molecular evolutionary genetics analysis across computing platforms. *Mol. Biol. Evol.* **35**, 1547-1549. doi:10.1093/molbev/msy096

Kuroiwa, T., Kuroiwa, H., Sakai, A., Takahashi, H., Toda, K. and Itoh, R. (1998). The division apparatus of plastids and mitochondria. *Int. Rev. Cytol.* **181**, 1-41. doi:10.1016/S0074-7696(08)60415-5

Kuroiwa, T., Miyagishima, S. Y., Matsunaga, S., Sato, N., Nozaki, H., Tanaka, K. and Misumi, O. eds. (2017). *Cyanidioschyzon Merolae: A New Model Eukaryote FOR Cell and Organelle Biology*. Singapore: Springer Singapore.

Langmead, B. and Salzberg, S. L. (2012). Fast gapped-read alignment with Bowtie 2. *Nat. Methods* **9**, 357-359. doi:10.1038/nmeth.1923

Lau, O. S. and Deng, X. W. (2012). The photomorphogenic repressors COP1 and DET1: 20 years later. *Trends Plant Sci.* **17**, 584-593. doi:10.1016/j.tplants.2012.05.004

Liao, Y., Smyth, G. K. and Shi, W. (2014). FeatureCounts: an efficient general purpose program for assigning sequence reads to genomic features. *Bioinformatics* **30**, 923-930. doi:10.1093/bioinformatics/btt656

Markwardt, M. L., Kremers, G. J., Kraft, C. A., Ray, K., Cranfill, P. J. C., Wilson, K. A., Day, R. N., Wachter, R. M., Davidson, M. W. and Rizzo, M. A. (2011). An improved cerulean fluorescent protein with enhanced brightness and reduced reversible photoswitching. *PLoS One* **6**, e17896. doi:10.1371/journal.pone.0017896

Martin, W. and Kowallik, K. (1999). Annotated english translation of mereschkowsky's 1905 paper 'Über natur und ursprung der chromatophoren impflanzenreiche. *Eur. J. Phycol.* **34**, 287-295. doi:10.1080/09670269910001736342

Matsuzaki, M., Misumi, O., Shin-i, T., Maruyama, S., Takahara, M., Miyagishima, S. Y., Mori, T., Nishida, K., Yagisawa, F., Nishida, K. et al. (2004). Genome sequence of the ultrasmall unicellular red alga *Cyanidioschyzon merolae* 10D. *Nature* **428**, 653-657. doi:10.1038/nature02398

Mereschkowsky, C. (1905). Über natur und ursprung der chromatophoren im pflanzenreiche. *Biol. Zent. Bl.* **25**, 593-604.

Minoda, A., Sakagami, R., Yagisawa, F., Kuroiwa, T. and Tanaka, K. (2004). Improvement of culture conditions and evidence for nuclear transformation by homologous recombination in a red alga, *Cyanidioschyzon merolae* 10D. *Plant Cell Physiol.* **45**, 667-671. doi:10.1093/pcp/pch087

Miyagishima, S. Y., Nishida, K., Mori, T., Matsuzaki, M., Higashiyama, T., Kuroiwa, H. and Kuroiwa, T. (2003). A plant-specific dynamin-related protein forms a ring at the chloroplast division site. *Plant Cell Online* **15**, 655-665. doi:10.1105/tpc.009373

Nagai, T., Ibata, K., Park, E. S., Kubota, M., Mikoshiba, K. and Miyawaki, A. (2002). A variant of yellow fluorescent protein with fast and efficient maturation for cell-biological applications. *Nat. Biotechnol.* **20**, 87-90. doi:10.1038/nbt0102-87

Naito, Y., Hino, K., Bono, H. and Ui-Tei, K. (2015). CRISPRdirect: Software for designing CRISPR/Cas guide RNA with reduced off-target sites. *Bioinformatics* **31**, 1120-1123. doi:10.1093/bioinformatics/btu743

Nishida, K., Takahara, M., Miyagishima, S. Y., Kuroiwa, H., Matsuzaki, M. and Kuroiwa, T. (2003). Dynamic recruitment of dynamin for final mitochondrial severance in a primitive red alga. *Proc. Natl. Acad. Sci. USA* **100**, 2146-2151. doi:10.1073/pnas.0436886100

Nishimasu, H., Ran, F. A., Hsu, P. D., Konermann, S., Shehata, S. I., Dohmae, N., Ishitani, R., Zhang, F. and Nureki, O. (2014). Crystal structure of Cas9 in complex with guide RNA and target DNA. *Cell* **156**, 935-949. doi:10.1016/j.cell.2014.02.001

Nozaki, H., Takano, H., Misumi, O., Terasawa, K., Matsuzaki, M., Maruyama, S., Nishida, K., Yagisawa, F., Yoshida, Y., Fujiwara, T. et al. (2007). A 100%-complete sequence reveals unusually simple genomic features in the hot-spring red alga *Cyanidioschyzon merolae*. *BMC Biol.* **5**, 28. doi:10.1186/1741-7007-5-28

Ohnuma, M., Yokoyama, Y., Inouye, T., Sekine, Y. and Tanaka, K. (2008). Polyethylene glycol (PEG)-mediated transient gene expression in a red alga, *Cyanidioschyzon merolae* 10D. *Plant Cell Physiol.* **49**, 117-120. doi:10.1093/pcp/pcm157

Öztürk, N., Song, S. H., Özgür, S., Selby, C. P., Morrison, L., Partch, C., Zhong, D. and Sancar, A. (2007). Structure and function of animal cryptochromes. *Cold Spring Harb. Symp. Quant. Biol.* **72**, 119-131. doi:10.1101/sqb.2007.72.015

Rizzini, L., Levine, D. C., Perelis, M., Bass, J., Peek, C. B. and Pagano, M. (2019). Cryptochromes-mediated inhibition of the CRL4 Cop1-complex assembly defines an evolutionary conserved signaling mechanism. *Curr. Biol.* **29**, 1954-1962.e4. doi:10.1016/j.cub.2019.04.073

Sander, J. D. and Joung, J. K. (2014). CRISPR-Cas systems for editing, regulating and targeting genomes. *Nat. Biotechnol.* **32**, 347-355. doi:10.1038/nbt.2842

Suzuki, K., Ehara, T., Osafune, T., Kuroiwa, H., Kawano, S. and Kuroiwa, T. (1994). Behavior of mitochondria, chloroplasts and their nuclei during the mitotic cycle in the ultramicroalga *Cyanidioschyzon merolae*. *Eur. J. Cell Biol.* **63**, 280-288.

Takahara, M., Takahashi, H., Matsunaga, S., Miyagishima, S., Takano, H., Sakai, A., Kawano, S. and Kuroiwa, T. (2000). A putative mitochondrial *ftsZ* gene is present in the unicellular primitive red alga *Cyanidioschyzon merolae*. *Mol. Gen. Genet.* **264**, 452-460. doi:10.1007/s004380000307

Takahashi, H., Takano, H., Yokoyama, A., Hara, Y., Toh-e, S., Akio, K. and Kuroiwa, T. (1995). from the primitive red alga *Cyanidioschyzon merolae*. *Curr. Genet.* **28**, 484-490. doi:10.1007/BF00310820

Wiese, C. and Zheng, Y. (2006). Microtubule nucleation: γ-tubulin and beyond. *J. Cell Sci.* **119**, 4143-4153. doi:10.1242/jcs.03226

Yagisawa, F., Fujiwara, T., Takemura, T., Kobayashi, Y., Sumiya, N., Miyagishima, S. Y., Nakamura, S., Imoto, Y., Misumi, O., Tanaka, K. et al. (2020). ESCRT machinery mediates cytokinetic abscission in the unicellular red alga *Cyanidioschyzon merolae*. *Front. Cell Dev. Biol.* **8**, 1-14. doi:10.3389/fcell.2020.00169

Yang, Q., Pando, B. F., Dong, G., Golden, S. S. and van Oudenaarden, A. (2010). Circadian gating of the cell cycle revealed in single cyanobacterial cells. *Science* **327**, 1522-1526. doi:10.1126/science.1181759

Yoshida, Y. and Mogi, Y. (2019). How do plastids and mitochondria divide? *Microscopy* **68**, 45-56. doi:10.1093/jmicro/dfy132

Yoshida, Y., Kuroiwa, H., Misumi, O., Yoshida, M., Ohnuma, M., Fujiwara, T., Yagisawa, F., Hirooka, S., Imoto, Y., Matsushita, K. et al. (2010). Chloroplasts divide by contraction of a bundle of nanofilaments consisting of polyglucan. *Science* **329**, 949-953. doi:10.1126/science.1190791

Yoshida, Y., Fujiwara, T., Imoto, Y., Yoshida, M., Ohnuma, M., Hirooka, S., Misumi, O., Kuroiwa, H., Kato, S., Matsunaga, S. et al. (2013). The kinesin-like protein TOP promotes Aurora localisation and induces mitochondrial, chloroplast and nuclear division. *J. Cell Sci.* **126**, 2392-2400. doi:10.1242/jcs.116798

Yoshida, Y., Kuroiwa, H., Shimada, T., Yoshida, M., Ohnuma, M., Fujiwara, T., Imoto, Y., Yagisawa, F., Nishida, K., Hirooka, S. et al. (2017). Glycosyltransferase MDR1 assembles a dividing ring for mitochondrial proliferation comprising polyglucan nanofilaments. *Proc. Natl. Acad. Sci. USA* **114**, 13284-13289. doi:10.1073/pnas.1715008114

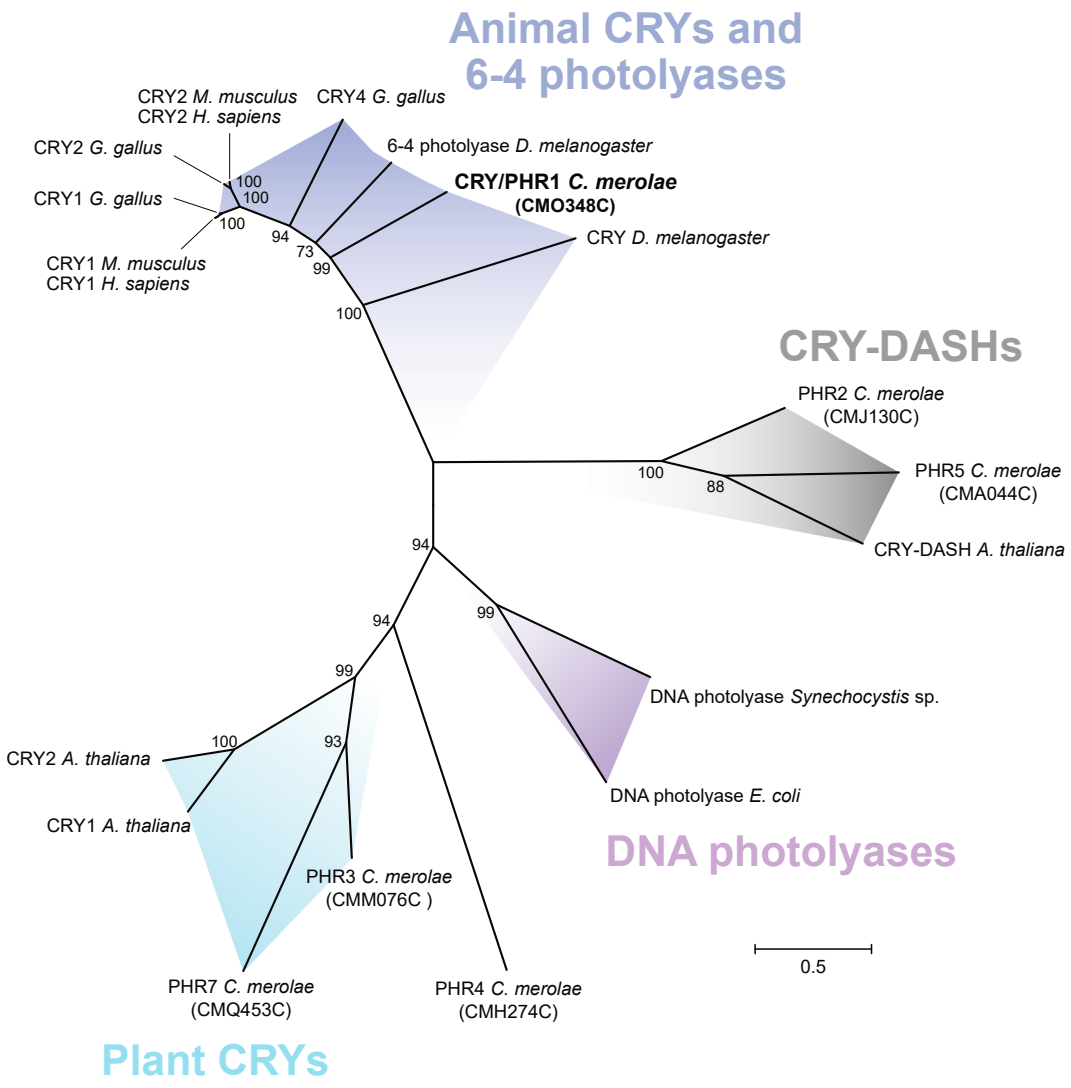

Fig. S1. Phylogenetic analysis of cryptochromes and photolyases. The phylogenetic tree was generated using the maximum likelihood method in MEGA X. The subfamilies of animal CRYs and 6-4 photolyases, CRY-DASHs, DNA photolyases, and plant CRYs are shown in blue, black, purple, and light blue, respectively. The numbers at each branch are local bootstrap values estimated using the neighbor-joining method from 1,000 replications.

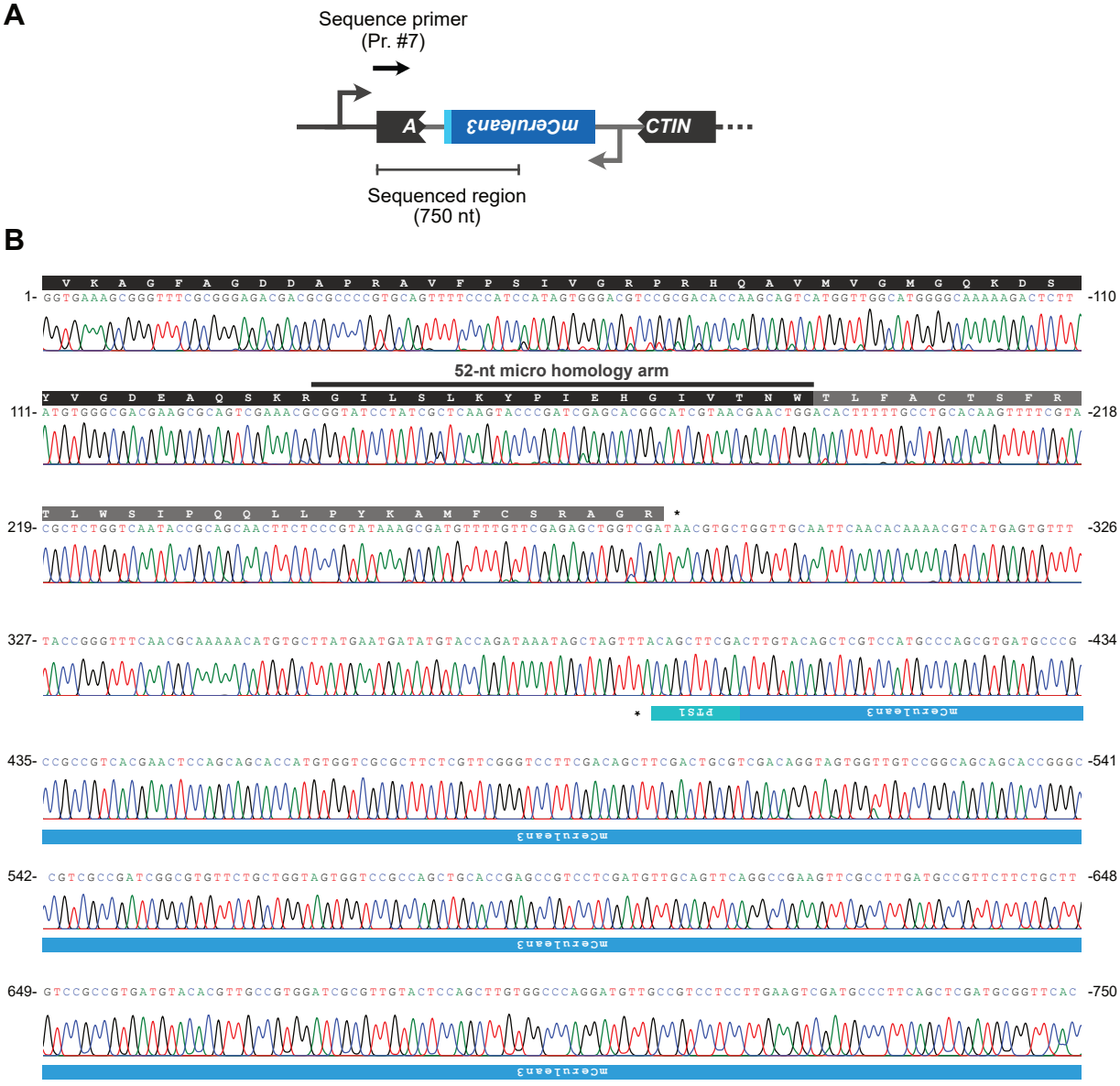

Fig. S2. DNA sequence at the insertion site of *perCerulean3* knocked into the *ACTIN* locus by CZON-cutter. (A) Schematic representation of the gene structure in the *ACTIN* knockout (*actin*) strain. (B) Sanger sequencing electropherogram of a transformed strain. The primer sequence (#7) is given in Table S4.

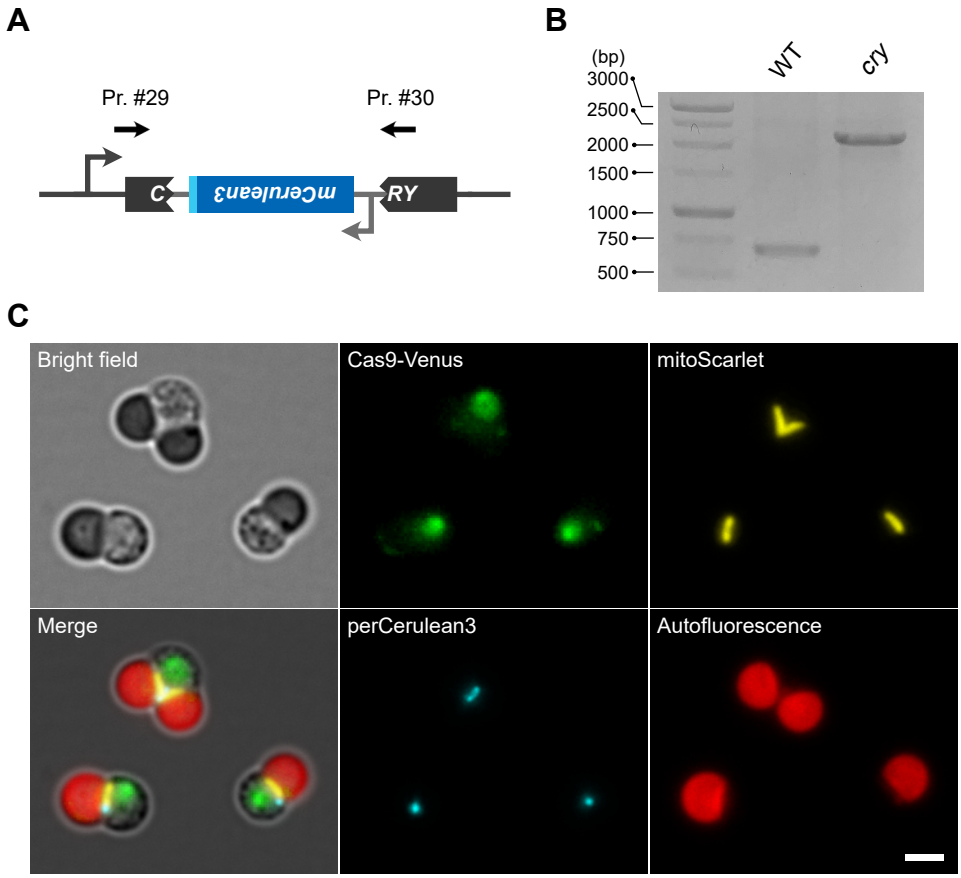

Fig. S3. Site-specific knock-in of an expression cassette encoding mCerulean3 fused to a peroxisomal targeting signal into the *CRY* locus by CZON-cutter. (A) Principle behind knocking in a fluorescent reporter expression cassette at the *CRY* locus. (B) Confirmation of the knock-in event at the *CRY* locus by PCR with primer sets #29 and #30 to amplify a fragment of the *CRY* locus. Primer sequences are given in Table S4. (C) Representative images of non-dividing and dividing cells of the *CRY* knockout (*cry*) strain. Green, Cas9-Venus fluorescence; yellow, mitoScarlet fluorescence; blue, perCerulean3 fluorescence; red, chlorophyll autofluorescence.

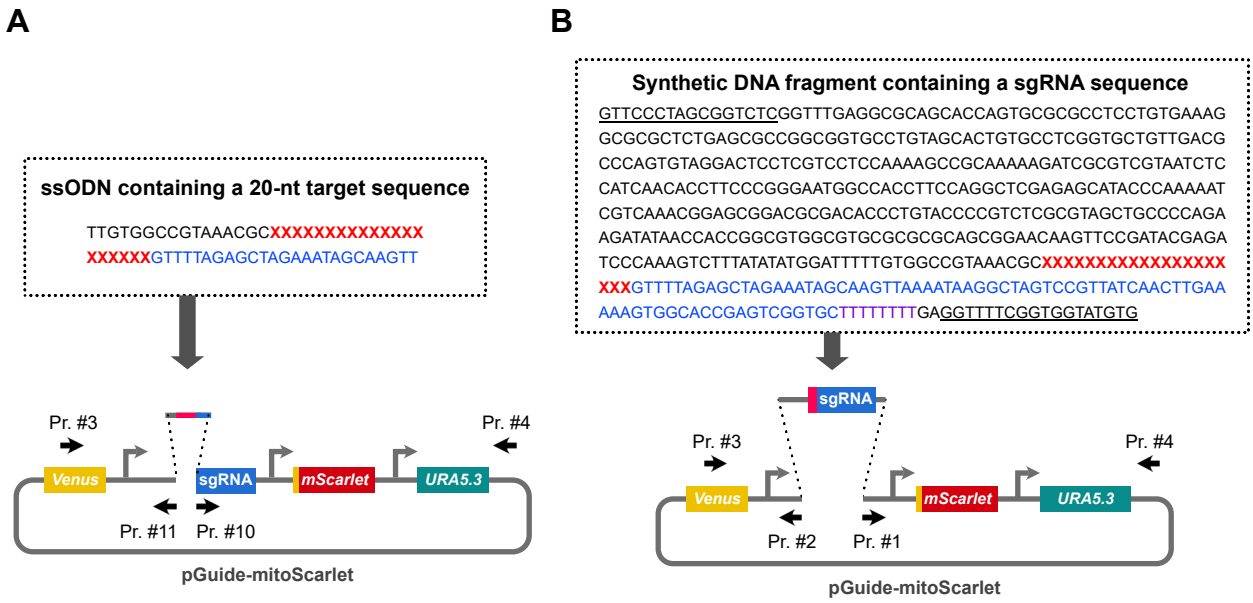

Fig. S4. Construction of the pGuide-mitoScarlet plasmid targeting a target locus. For construction of a given single guide RNA (sgRNA), the target sequence can be introduced by following two procedures. (A) A single-stranded oligodeoxynucleotide containing a 20-nt target sequence is combined with a DNA fragment amplified by PCR using primers #10 and #11. (B) A synthetic DNA fragment containing the U6 promoter sequence, a 20-nt target sequence, a sgRNA scaffold sequence, and a transcription termination signal are combined with a DNA fragment amplified by PCR using primers #1 and #2. The 20-nt target sequence is shown as “X” in red. The sgRNA scaffold is shown in blue and the transcription termination signal in purple. Sequences for recombination are underlined. Primer sequences are given in Table S4. See methods for details.

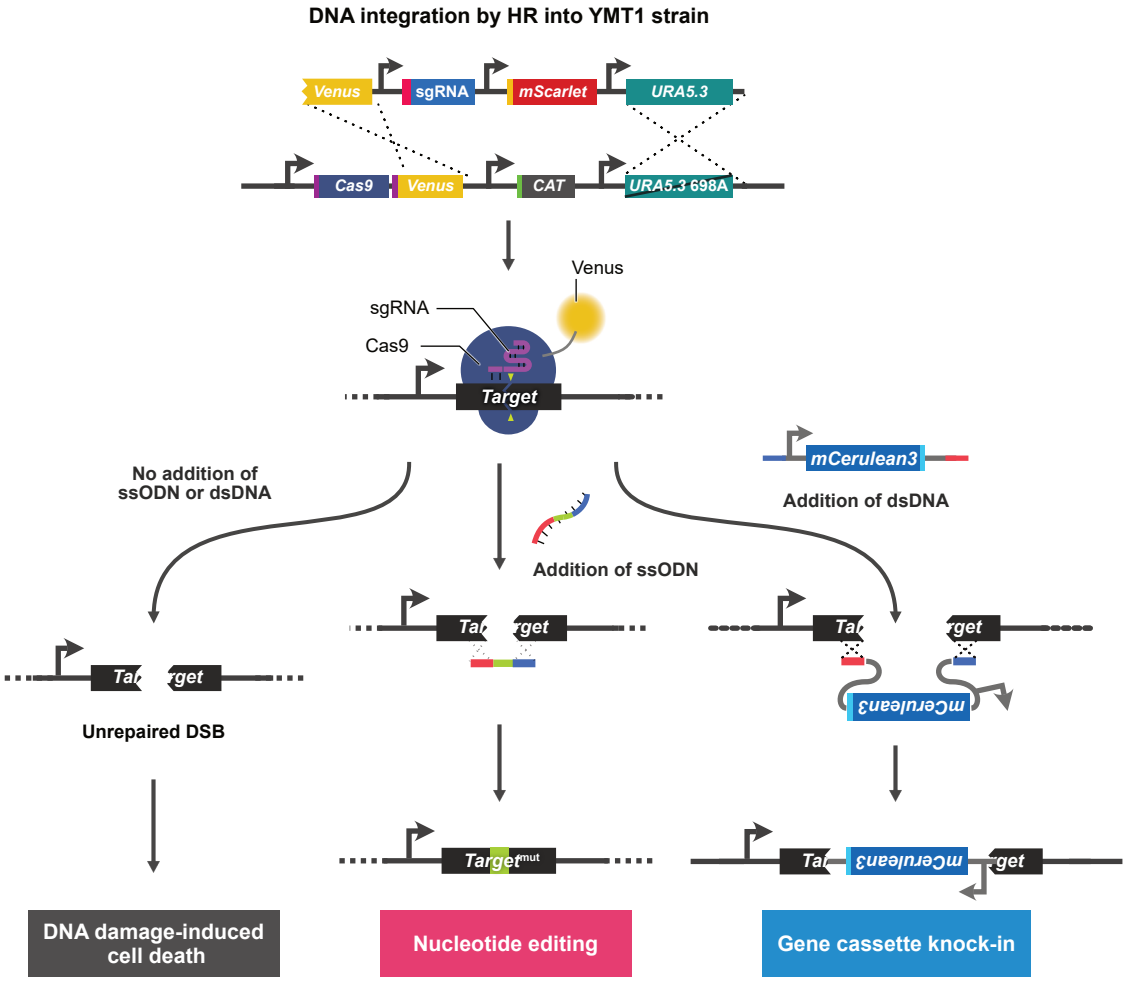

Fig. S5. Schematic flowchart of CZON-cutter. For genome editing and gene knock-in, a synthetic DNA fragment containing a single guide RNA (sgRNA) with a specific target sequence was synthesized and then assembled with a linearized pGuide-mitoScarlet vector. A PCR amplicon containing the sgRNA, *mitoScarlet*, and *URA5.3* cassettes was mixed with an 80-nt single-stranded oligodeoxynucleotide (ssODN; for nucleotide modification) or double-stranded DNA (dsDNA; for gene knock-in) and introduced into YMT1 cells. A transformed cell that does not take in the ssODN or dsDNA and does not undergo gene editing will die from DNA damage-induced cell death.

Table S1. Summary of datasets for synchronization of the wild-type (WT) and *CRY* knockout (*ko*) strains.

Strain	Light quality, photon flux density (µmol m^{-2} s^{-1})	Sample number	Number of non-dividing cells	Number of dividing cells	Total number of cells	Percentage of dividing cells	Average (%)	Standard deviation (%)	*p* value (Student's *t*-test)
WT	White Blue: 9.0 Green: 15.4 Red: 8.8	1	88	95	183	51.9	53.75	1.55	0.00011
		2	62	78	140	55.7			
		3	96	111	207	53.6			
ko		1	190	68	258	26.4	28.2	2.4	
		2	158	73	231	31.6			
		3	181	66	247	26.7			

Strain	Light quality, photon flux density (µmol m^{-2} s^{-1})	Sample number	Number of non-dividing cells	Number of dividing cells	Total number of cells	Percentage of dividing cells	Average (%)	Standard deviation (%)	*p* value (Student's *t*-test)
WT	Blue and Red Blue: 15.4 Green: 0.8 Red: 15.4	1	179	220	399	55.1	53.6	1.7	0.00078
		2	115	121	236	51.3			
		3	51	61	112	54.5			
ko		1	300	228	528	43.2	42.3	1.2	
		2	138	94	232	40.5			
		3	124	94	218	43.1			

Strain	Light quality, photon flux density (µmol m^{-2} s^{-1})	Sample number	Number of non-dividing cells	Number of dividing cells	Total number of cells	Percentage of dividing cells	Average (%)	Standard deviation (%)	*p* value (Student's *t*-test)
WT	Red Blue: 0.1 Green: 0.2 Red: 31.5	1	152	52	204	25.5	22.4	2.19	0.49304
		2	123	32	155	20.6			
		3	131	35	166	21.1			
ko		1	144	22	166	13.3	22.5	6.72	
		2	83	28	111	25.2			
		3	181	74	255	29.0			

Table S2. Top 50 upregulated and downregulated genes between the *CRY* knockout strain and the wi ld-type strain.

Top 50 upregulated genes

#	Gene ID	Annotation	Gene length (bp)	Read count (WT)	Read count (*ko*)	TPM (WT)	TPM (*ko*)	Log_2 WT	Log_2 KO	Average	LogFC (*ko*/WT)
1	CMC002C	similar to hedgehog protein	2,331	432	1,204	133.4	357.5	7.1	8.5	7.8	1.4
2	CMB088C	probable nucleotide binding protein Maf	621	742	1,635	860.2	1,822.5	9.7	10.8	10.3	1.1
3	CMB086C	hypothetical protein	540	707	1,515	942.6	1,942.1	9.9	10.9	10.4	1.0
4	CMB085C	hypothetical protein	2,025	296	633	105.2	216.4	6.7	7.8	7.2	1.0
5	CMB087C	hypothetical protein, conserved	2,814	1,321	2,707	338.0	665.9	8.4	9.4	8.9	1.0
6	CMB081C	hypothetical protein, conserved	2,655	6,615	12,981	1793.7	3,384.5	10.8	11.7	11.3	0.9
7	CMB082C	similar to JEMMA protein	2,202	1,975	3,845	645.7	1,208.7	9.3	10.2	9.8	0.9
8	CMB083C	chaperonin containing TCP1, subunit 3 (gamma)	1,677	1,566	2,892	672.3	1,193.7	9.4	10.2	9.8	0.8
9	CMD002C	similar to trefoil factor	3,282	145	253	31.8	53.4	5.0	5.7	5.4	0.7
10	CMW053C	[mt] 30S ribosomal protein S12	369	450	769	878.0	1,442.6	9.8	10.5	10.1	0.7
11	CMK045C	pseudouridine synthase 3	1,401	3,598	6,121	1848.9	3,024.3	10.9	11.6	11.2	0.7
12	CMI002C	copper-containing amine oxidase	1,899	809	1,337	306.7	487.4	8.3	8.9	8.6	0.7
13	CMM057C	hypothetical protein	1,275	125	205	70.6	111.3	6.1	6.8	6.5	0.7
14	CMK046C	uridine 5'-monophosphate synthase (UMP synthase)	1,389	4,028	6,569	2087.7	3,273.7	11.0	11.7	11.4	0.6
15	CMN328C	probable phosphate/phosphoenolpyruvate translocator precursor	1,182	401	641	244.2	375.4	7.9	8.6	8.2	0.6
16	CMR293C	hypothetical protein	690	176	281	183.6	281.9	7.5	8.1	7.8	0.6
17	CMI286C	hypothetical protein	2,784	771	1,216	199.4	302.3	7.6	8.2	7.9	0.6
18	CML108C	hypothetical protein, conserved	2,139	322	505	108.4	163.4	6.8	7.4	7.1	0.6
19	CMW007C	[mt] cytochrome B	1,146	770	1,196	483.7	722.4	8.9	9.5	9.2	0.6
20	CMQ113C	similar to translationally controlled tumor protein (TCTP) (p23)	507	548	840	778.1	1,146.9	9.6	10.2	9.9	0.6

#	Gene ID	Annotation	Gene length (bp)	Read count (WT)	Read count (*ko*)	TPM (WT)	TPM (*ko*)	Log_2 WT	Log_2 KO	Average	LogFC (*ko*/WT)
21	CMF130C	hypothetical protein	1,827	261	384	102.8	145.5	6.7	7.2	6.9	0.5
22	CMT448C	hypothetical protein	855	105	154	88.4	124.7	6.5	7.0	6.7	0.5
23	CMO348C	Mammalian CRY1	1,557	734	1,076	339.4	478.4	8.4	8.9	8.7	0.5
24	CMI306C	mitochondrial ribosomal protein S1 precursor	1,062	2,113	3,093	1432.4	2,016.0	10.5	11.0	10.7	0.5
25	CMR047C	hypothetical protein	843	272	393	232.3	322.7	7.9	8.3	8.1	0.5
26	CMS191C	similar to methyltransferase	654	1,964	2,793	2162.0	2,956.2	11.1	11.5	11.3	0.5
27	CMT597C	heat shock transcription factor	1,350	447	634	238.4	325.1	7.9	8.3	8.1	0.4
28	CMO066C	cytochrome b6/f complex iron-sulfur subunit precursor	720	433	614	433.0	590.3	8.8	9.2	9.0	0.4
29	CMP092C	hypothetical protein	555	628	879	814.6	1,096.3	9.7	10.1	9.9	0.4
30	CMD051C	hypothetical protein	1,359	1,526	2,100	808.4	1,069.7	9.7	10.1	9.9	0.4
31	CMQ259C	hypothetical protein	429	285	391	478.3	630.9	8.9	9.3	9.1	0.4
32	CMT349C	hypothetical protein	336	581	797	1244.9	1,642.0	10.3	10.7	10.5	0.4
33	CMP030C	probable chromatin assembly factor 1 subunit B	1,569	177	238	81.2	105.0	6.3	6.7	6.5	0.4
34	CMR042C	similar to carbonyl reductase	855	3,999	5,375	3367.2	4,351.7	11.7	12.1	11.9	0.4
35	CMT300C	similar to origin recognition complex subunit 4	1,722	240	322	100.3	129.4	6.6	7.0	6.8	0.4
36	CMT333C	similar to inorganic phosphate transporter	1,956	245	328	90.2	116.1	6.5	6.9	6.7	0.4
37	CMQ224C	heat shock protein of Hsp90 family	2,118	19,722	26,237	6703.6	8,575.0	12.7	13.1	12.9	0.4
38	CML030C	DnaJ (Hsp40) homolog, subfamily A	1,281	10,274	13,588	5774.0	7,342.6	12.5	12.8	12.7	0.3
39	CMT538C	hypothetical protein	4,101	1,260	1,663	221.2	280.7	7.8	8.1	8.0	0.3
40	CMT049C	hypothetical protein	1,578	479	632	218.5	277.2	7.8	8.1	7.9	0.3
41	CMR165C	sigma subunit for chloroplast RNA polymerase	1,947	7,267	9,586	2687.0	3,408.1	11.4	11.7	11.6	0.3
42	CME192C	uridine kinase	1,284	242	319	135.7	172.0	7.1	7.4	7.3	0.3
43	CMC188C	L-lactate dehydrogenase	1,062	669	881	453.5	574.2	8.8	9.2	9.0	0.3

Journal of Cell Science • Supplementary information

#	Gene ID	Annotation	Gene length (bp)	Read count (WT)	Read count (*ko*)	TPM (WT)	TPM (*ko*)	Log_2 WT	Log_2 KO	Average	LogFC (*ko*/WT)
44	CME023C	fusion protein of phosphoribosylaminoimidazole carboxylase and phosphoribosylaminoimidazole-succinocarboxamide synthase, chloroplast or mitochondrial precursor	1,791	6,914	9,101	2779.2	3,517.5	11.4	11.8	11.6	0.3
45	CMA145C	L-lactate dehydrogenase	1,062	2,085	2,743	1413.4	1,787.9	10.5	10.8	10.6	0.3
46	CMD135C	ATP-binding cassette, sub-family G	2,475	11,268	14,696	3277.6	4,110.3	11.7	12.0	11.8	0.3
47	CMT087C	similar to DNA replication licensing factor MCM8	2,970	354	461	85.8	107.4	6.4	6.7	6.6	0.3
48	CMO111C	outer mitochondrial membrane protein porin	915	1,706	2,219	1342.3	1,678.7	10.4	10.7	10.6	0.3
49	CMD134C	ATP-binding cassette, sub-family G	2,286	9,095	11,824	2864.3	3,580.4	11.5	11.8	11.6	0.3
50	CMG131C	hypothetical protein	966	424	551	316.0	394.8	8.3	8.6	8.5	0.3

Top 50 downregulated genes

#	Gene ID	Annotation	Gene length (bp)	Read count (WT)	Read count (*ko*)	TPM (WT)	TPM (*ko*)	Log_2 WT	Log_2 *ko*	Average	LogFC (*ko*/WT)
1	CME121C	probable kynurenine aminotransferase	1,632	1,558	720	687.3	305.4	9.4	8.3	8.8	–1.2
2	CMD163C	probable molybdopterin converting factor small subunit MoaD	261	836	579	2,306.0	1,535.6	11.2	10.6	10.9	–0.6
3	CMP170C	similar to formamidopyrimidine-DNA glycosylase	780	324	238	299.0	211.2	8.2	7.7	8.0	–0.5
4	CMG100C	hypothetical protein	1,617	181	134	80.6	57.4	6.3	5.8	6.1	–0.5
5	CMP240C	retroelement	372	437	329	845.7	612.2	9.7	9.3	9.5	–0.5
6	CMV040C	[pt] ORF105	315	193	147	441.1	323.0	8.8	8.3	8.6	–0.4
7	CMR137C	similar to developmental gene, multi-sex-combs	1,530	1,381	1,060	649.8	479.6	9.3	8.9	9.1	–0.4
8	CMC047C	hypothetical protein, conserved	993	148	114	107.3	79.5	6.7	6.3	6.5	–0.4
9	CMQ139C	hypothetical protein, conserved	2,421	940	725	279.5	207.3	8.1	7.7	7.9	–0.4
10	CMQ155C	hypothetical protein	1,518	181	140	85.8	63.8	6.4	6.0	6.2	–0.4
11	CMV049C	[pt] ORF73	216	138	107	459.9	342.9	8.8	8.4	8.6	–0.4
12	CMD073C	hypothetical protein	357	446	349	899.4	676.7	9.8	9.4	9.6	–0.4
13	CMC022C	probable endoplasmic reticulum oxidoreductin 1-Lbeta (ERO1-L)	1,575	1,101	862	503.3	378.9	9.0	8.6	8.8	–0.4
14	CMC142C	hypothetical protein	993	284	224	205.9	156.2	7.7	7.3	7.5	–0.4

#	Gene ID	Annotation	Gene length (bp)	Read count (WT)	Read count (*ko*)	TPM (WT)	TPM (*ko*)	Log_2 WT	Log_2 *ko*	Average	LogFC (*ko*/WT)
15	CMN138C	probable AAA protein spastin	1,656	887	702	385.6	293.4	8.6	8.2	8.4	–0.4
16	CMT542C	similar to phosphoserine phosphatase	648	315	252	350.0	269.2	8.5	8.1	8.3	–0.4
17	CMF088C	hypothetical protein	1,143	1,473	1,182	927.8	715.8	9.9	9.5	9.7	–0.4
18	CMP321C	similar to anaphase-promoting complex subunit 10 (APC10)	1,173	595	478	365.2	282.1	8.5	8.1	8.3	–0.4
19	CMT450C	similar to nuclear transport factor 2	393	330	266	604.5	468.5	9.2	8.9	9.1	–0.4
20	CMP182C	hypothetical protein	1,143	875	711	551.1	430.6	9.1	8.8	8.9	–0.4
21	CMR316C	hypothetical protein	1,131	6,860	5,606	4,366.6	3,431.1	12.1	11.7	11.9	–0.3
22	CMP061C	hypothetical protein	1,008	1,159	954	827.8	655.1	9.7	9.4	9.5	–0.3
23	CMP293C	hypothetical protein, conserved	504	356	294	508.5	403.8	9.0	8.7	8.8	–0.3
24	CMN019C	probable inorganic phosphate transporter	1,914	10,345	8,553	3,891.1	3,093.3	11.9	11.6	11.8	–0.3
25	CMC078C	hypothetical protein, conserved	384	371	307	695.5	553.4	9.4	9.1	9.3	–0.3
26	CMT563C	hypothetical protein	882	431	357	351.8	280.2	8.5	8.1	8.3	–0.3
27	CME183C	hypothetical protein	522	10,458	8,690	14,423.2	11,523.8	13.8	13.5	13.7	–0.3
28	CMT031C	hypothetical protein	663	431	359	468.0	374.8	8.9	8.6	8.7	–0.3
29	CMH150C	hypothetical protein, conserved	744	487	408	471.2	379.6	8.9	8.6	8.7	–0.3
30	CMS018C	thioredoxin-like U5 snRNP component dim1	423	364	305	619.5	499.1	9.3	9.0	9.1	–0.3
31	CMQ121C	hypothetical protein, conserved	564	453	380	578.2	466.4	9.2	8.9	9.0	–0.3
32	CMT114C	similar to ribonuclease PH	882	533	448	435.1	351.6	8.8	8.5	8.6	–0.3
33	CMJ137C	hypothetical protein, conserved	516	201	169	280.4	226.7	8.1	7.8	8.0	–0.3
34	CMV001C	[pt] ABC transporter for iron-sulfur cluster formation (sufB)	1,395	151	127	77.9	63.0	6.3	6.0	6.1	–0.3
35	CMQ466C	similar to 4-aminobutyrate aminotransferase (GABA aminotransferase)	609	120	101	141.9	114.8	7.1	6.8	7.0	–0.3
36	CMO085C	hypothetical protein	492	1,052	887	1,539.3	1,248.0	10.6	10.3	10.4	–0.3
37	CMN051C	similar to 6-pyruvoyltetrahydropterin synthase	675	359	303	382.9	310.7	8.6	8.3	8.4	–0.3
38	CMR072C	hypothetical protein	360	579	490	1,157.9	942.2	10.2	9.9	10.0	–0.3

#	Gene ID	Annotation	Gene length (bp)	Read count (WT)	Read count (*ko*)	TPM (WT)	TPM (*ko*)	Log_2 WT	Log_2 *ko*	Average	LogFC (*ko*/WT)
39	CML249C	probable 8-oxoguanine-DNA-glycosylase	1,206	3,225	2,735	1,925.2	1,569.8	10.9	10.6	10.8	–0.3
40	CMG014C	similar to G10 protein	702	298	253	305.6	249.5	8.3	8.0	8.1	–0.3
41	CMH224C	mitochondrial ribosomal protein L13 precursor	678	704	598	747.5	610.5	9.5	9.3	9.4	–0.3
42	CMP220C	similar to actin-binding protein, profilin	591	134	114	163.2	133.5	7.4	7.1	7.2	–0.3
43	CMR459C	similar to fructosamine 3 kinase	924	691	588	538.4	440.5	9.1	8.8	8.9	–0.3
44	CMC172C	hypothetical protein, conserved	1,506	1,017	868	486.2	399.0	8.9	8.6	8.8	–0.3
45	CMK039C	photoregulatory zinc-finger protein COP1	2,565	3,206	2,738	899.8	738.9	9.8	9.5	9.7	–0.3
46	CMT267C	similar to glycosyl transferase	1,350	644	550	343.4	282.0	8.4	8.1	8.3	–0.3
47	CMO069C	hypothetical protein	399	775	662	1,398.3	1,148.5	10.4	10.2	10.3	–0.3
48	CMV089C	[pt] photosystem II protein W	327	151	129	332.4	273.1	8.4	8.1	8.2	–0.3
49	CMP078C	probable beta-galactosidase	2,331	820	701	253.3	208.2	8.0	7.7	7.8	–0.3
50	CMJ262C	MDR1	2,100	1,429	1,223	489.9	403.1	8.9	8.7	8.8	–0.3

Table S3

Evaluation of CRISPR-Cas9 target sites for *CRY*, *ACTIN*, *MDR1*, and *TUBG* by the CRISPRdirect online tool. Target sequences for CRISPR are shown in bold, and PAM sequences are shown in italics.

Target gene	Start	End	Strand	Sequence	GC (%)	Tm (ºC)	TTTT	Hit_20mer	Hit_12mer	Hit_8mer
CMO348C *CRY*	232	254	+	**tctagactgtttgtgcttcg***ggg*	45	68.62	0	1	1	116
CMM237C *ACTIN*	239	261	+	**gggatgatatggaaaag atc***tgg*	40	65.77	0	1	1	28
CMJ262C *MDR1*	254	276	–	**gggctcgtgggaaagta cgg***cgg*	65	79.45	0	1	1	19
CMN304C *TUBG*	863	885	+	**cgtacagccaccaagat ctg***cgg*	55	73.39	0	1	1	18

Table S4. Primers and synthetic DNA fragments used in this study. Sequences for recombination are underlined. An additional nucleotide and inserted stop codons (TGA) are shown in bold. The complete nucleotide sequence of the synthetic DNA fragments for single-guide RNAs (sgRNAs) targeting *CRY*, *ACTIN*, and *MDR1* are listed as #16 to #18. Target sequences are shown in red. sgRNA scaffold sequences and transcription termination signals are shown in blue and purple, respectively.

DNA #	Sequence	Description
1	GGTTTTCGGTGGTATGTGATTTACAGCGAAAC	For PCR amplification of pGuide-mitoScarlet vector to assemble with a synthetic DNA
2	GAGACCGCTAGGGAACGTTCGG	
3	CGGCGATGTCAACGGTCACAAATTCTC	For transformation of DNA fragments containing sgRNA, *mitoScarlet*, and *URA5.3* gene cassettes
4	AGCAGCTGACTGTATCTCTATTCTTAGGAATCC	
5	GGATGATCCTCGGGGGAGATGCGCAACTCGTTGTAAAAAGTGT GGTACCACGACGAGAACGTATAAGGAGTGCG	For PCR amplification of the *perCerulean3* gene cassette for the knock-in in the *ACTIN* locus
6	CGGTATCCTATCGCTCAAGTACCCGATCGAGCACGGCATCGTA ACGAACTGGACACTTTTTGCCTGCACAAGTTTTCG	
7	ATGACAGAGGAGGAAATAACAGCTCTTGTG	For PCR amplification of *ACTIN* ORF
8	GAAACATTTGCGGTGTACCACAGAG	
9	TTGTGGCCGTAAACGC**G***CGTACAGCCACCAAGATCTG*GTTTTA GAGCTAGAAATAGCAAGTT	For construction of pGuide-*TUBG*$_{863\text{-}885}$-mitoScarlet
10	GTTTTAGAGCTAGAAATAGCAAGTTAAAATAAGGCTAG	For PCR amplification of pGuide-mitoScarlet vector to assemble with a ssODN
11	GCGTTTACGGCCACAAAAATCCATATATAAAGAC	
12	AGGAGTTCCACTCGGGAGCTTTTCTTGAGAGCTTTGACAACGAA GGCGTC**TGA**ACACTTTTTGCCTGCACAAGTTTTCG	For PCR amplification of the *perCerulean3* gene cassette for the knock-in in the *MDR1* locus
13	TCAGTATACGAGTGACGTAGGCTTTCGTCGCTGTTCCACGAGC GGGCTCGCGACGAGAACGTATAAGGAGTGCG	
14	CGATGGTCATGGCAGCGTCGACCACGACGATGCGATTCCCAGC GTACAGC**TGA**ACACTTTTTGCCTGCACAAGTTTTCG	For PCR amplification of the *perCerulean3* gene cassette for the knock-in in the *TUBG* locus
15	CTTGCCACCAGAAAGTGACAAGGCGGGAGCGGCACCAATGTAG ACATCAGCGACGAGAACGTATAAGGAGTGCG	
16	GTTCCCTAGCGGTCTCGGTTTGAGGCGCAGCACCAGTGCGCGC CTCCTGTGAAAGGCGCGCTCTGAGCGCCGGCGGTGCCTGTAG CACTGTGCCTCGGTGCTGTTGACGCCCAGTGTAGGACTCCTCG TCCTCCAAAAGCCGCAAAAAGATCGCGTCGTAATCTCCATCAAC ACCTTCCCGGGAATGGCCACCTTCCAGGCTCGAGAGCATACCC AAAAATCGTCAAACGGAGCGGACGCGACACCCTGTACCCCGTC TCGCGTAGCTGCCCCAGAAGATATAACCACCGGCGTGGCGTGC GCGCGCAGCGGAACAAGTTCCGATACGAGATCCCAAAGTCTTTA TATATGGATTTTTGTGGCCGTAAACGCGTCTAGACTGTTTGTGCT TCGGTTTTAGAGCTAGAAATAGCAAGTTAAAATAAGGCTAGTCCG TTATCAACTTGAAAAAGTGGCACCGAGTCGGTGCTTTTTTTTGAG GTTTTCGGTGGTATGTG	Synthetic DNA for sgRNA targeting 232–254 bp of the *CRY* locus
17	GTTCCCTAGCGGTCTCGGTTTGAGGCGCAGCACCAGTGCGCGC CTCCTGTGAAAGGCGCGCTCTGAGCGCCGGCGGTGCCTGTAG CACTGTGCCTCGGTGCTGTTGACGCCCAGTGTAGGACTCCTCG TCCTCCAAAAGCCGCAAAAAGATCGCGTCGTAATCTCCATCAAC ACCTTCCCGGGAATGGCCACCTTCCAGGCTCGAGAGCATACCC AAAAATCGTCAAACGGAGCGGACGCGACACCCTGTACCCCGTC TCGCGTAGCTGCCCCAGAAGATATAACCACCGGCGTGGCGTGC GCGCGCAGCGGAACAAGTTCCGATACGAGATCCCAAAGTCTTTA TATATGGATTTTTGTGGCCGTAAACGCGGGATGATATGGAAAAGA TCGTTTTAGAGCTAGAAATAGCAAGTTAAAATAAGGCTAGTCCGT TATCAACTTGAAAAAGTGGCACCGAGTCGGTGCTTTTTTTTGAG GTTTTCGGTGGTATGTG	Synthetic DNA for sgRNA targeting 239–261 bp of the *ACTIN* locus

DNA #	Sequence	Description
18	GTTCCCTAGCGGTCTCGGTTTGAGGCGCAGCACCAGTGCGCGC CTCCTGTGAAAGGCGCGCTCTGAGCGCCGGCGGTGCCTGTAG CACTGTGCCTCGGTGCTGTTGACGCCCAGTGTAGGACTCCTCG TCCTCCAAAAGCCGCAAAAAGATCGCGTCGTAATCTCCATCAAC ACCTTCCCGGGAATGGCCACCTTCCAGGCTCGAGAGCATACCC AAAAATCGTCAAACGGAGCGGACGCGACACCCTGTACCCCGTC TCGCGTAGCTGCCCCAGAAGATATAACCACCGGCGTGGCGTGC GCGCGCAGCGGAACAAGTTCCGATACGAGATCCCAAAGTCTTTA TATATGGATTTTTGTGGCCGTAAACGCGGGCTCGTGGGAAAGTA CGGGTTTTAGAGCTAGAAATAGCAAGTTAAAATAAGGCTAGTCCG TTATCAACTTGAAAAAGTGGCACCGAGTCGGTGCTTTTTTTTGAG GTTTTCGGTGGTATGTG	Synthetic DNA for sgRNA targeting 254–276 bp of the *MDR1* locus
19	GTTTCTTCGTTCGTTGACCATGGTGTCGAAGGGCGAGGAGC	For PCR amplification of *perCerulean3* ORF
20	GCTAGTTTACAGCTTCGACTTGTACAGCTCGTCCATGCCCAG	
21	ATTGACGCGTATTGGGATCGACGAGAACGTATAAGGAGTGCG	For PCR amplification of a *ApcC* promoter sequence
22	GGTCAACGAACGAAGAAACACAGAGAACAAAG	
23	TCGAAGCTGTAAACTAGCTATTTATCTGGTACATATCATTCATAA GCAC	For PCR amplification of a *TUBB* 3′ UTR
24	CGCGCCATTGGGATACACTTTTTGCCTGCACAAGTTTTCG	
25	ATCCCAATGGCGCGCCGAGCTTG	For PCR amplification of pUC57 vector DNA
26	ATCCCAATACGCGTCAATTCACTGGC	
27	TTCTGCTAGAGTGCTTACAGGATCTGGACCAGCAACTTCGCAAG CTG**TGA**ACACTTTTTGCCTGCACAAGTTTTCG	For PCR amplification of the *perCerulean3* gene cassette for the knock-in in the *CRY* locus
28	GCGTATGATACTTTCGGAAAAAGACGGGTAGTTGCTCCAGCGG ATTGCCCGACGAGAACGTATAAGGAGTGCG	
29	ATGTGGGTCATCTTGACCATGGCAAG	For PCR amplification of *CRY* ORF
30	CGTAAAAAGTTCTCCATGCGCCTGAG	

ORF, open reading frame; ssODN, single-stranded oligodeoxynucleotide; UTR, untranslated region.

Table S5. Complete amino acid sequence of Cas9-Venus. *Streptococcus pyogenes* Cas9 and Venus are shown in blue and orange, respectively. The nuclear localization sequences are shown in purple and bold font, the 3× FLAG tag in green, and the 3× HA tag in red and italics.

Cas9-Venus (1,689 aa)

MDYKDHDGDYKDHDIDYKDDDDKMA**PKKKRKV**GIHGVPAADKKYSIGLDIGTNSVGWAVI
TDEYKVPSKKFKVLGNTDRHSIKKNLIGALLFDSGETAEATRLKRTARRRYTRRKNRICYLQ
EIFSNEMAKVDDSFFHRLEESFLVEEDKKHERHPIFGNIVDEVAYHEKYPTIYHLRKKLVDST
DKADLRLIYLALAHMIKFRGHFLIEGDLNPDNSDVDKLFIQLVQTYNQLFEENPINASGVDAK
AILSARLSKSRRLENLIAQLPGEKKNGLFGNLIALSLGLTPNFKSNFDLAEDAKLQLSKDTYD
DDLDNLLAQIGDQYADLFLAAKNLSDAILLSDILRVNTEITKAPLSASMIKRYDEHHQDLTLLK
ALVRQQLPEKYKEIFFDQSKNGYAGYIDGGASQEEFYKFIKPILEKMDGTEELLVKLNREDL
LRKQRTFDNGSIPHQIHLGELHAILRRQEDFYPFLKDNREKIEKILTFRIPYYVGPLARGNSR
FAWMTRKSEETITPWNFEEVVDKGASAQSFIERMTNFDKNLPNEKVLPKHSLLYEYFTVYN
ELTKVKYVTEGMRKPAFLSGEQKKAIVDLLFKTNRKVTVKQLKEDYFKKIECFDSVEISGVE
DRFNASLGTYHDLLKIIKDKDFLDNEENEDILEDIVLTLTLFEDREMIEERLKTYAHLFDDKVM
KQLKRRRYTGWGRLSRKLINGIRDKQSGKTILDFLKSDGFANRNFMQLIHDDSLTFKEDIQK
AQVSGQGDSLHEHIANLAGSPAIKKGILQTVKVVDELVKVMGRHKPENIVIEMARENQTTQ
KGQKNSRERMKRIEEGIKELGSQILKEHPVENTQLQNEKLYLYYLQNGRDMYVDQELDINR
LSDYDVDHIVPQSFLKDDSIDNKVLTRSDKNRGKSDNVPSEEVVKKMKNYWRQLLNAKLIT
QRKFDNLTKAERGGLSELDKAGFIKRQLVETRQITKHVAQILDSRMNTKYDENDKLIREVKV
ITLKSKLVSDFRKDFQFYKVREINNYHHAHDAYLNAVVGTALIKKYPKLESEFVYGDYKVYD
VRKMIAKSEQEIGKATAKYFFYSNIMNFFKTEITLANGEIRKRPLIETNGETGEIVWDKGRDF
ATVRKVLSMPQVNIVKKTEVQTGGFSKESILPKRNSDKLIARKKDWDPKKYGGFDSPTVAY
SVLVVAKVEKGKSKKLKSVKELLGITIMERSSFEKNPIDFLEAKGYKEVKKDLIIKLPKYSLFE
LENGRKRMLASAGELQKGNELALPSKYVNFLYLASHYEKLKGSPEDNEQKQLFVEQHKHY
LDEIIEQISEFSKRVILADANLDKVLSAYNKHRDKPIREQAENIIHLFTLTNLGAPAAFKYFDTT
IDRKRYTSTKEVLDATLIHQSITGLYETRIDLSQLGGDEGA**PKKKRKV**GSSVVSKGEELFTG
VVPILVELDGDVNGHKFSVSGEGEGDATYGKLTLKLICTTGKLPVPWPTLVTTLGYGLQCFA
RYPDHMKQHDFFKSAMPEGYVQERTIFFKDDGNYKTRAEVKFEGDTLVNRIELKGIDFKE
DGNILGHKLEYNYNSHNVYITADKQKNGIKANFKIRHNIEDGGVQLADHYQQNTPIGDGPV
LLPDNHYLSYQSALSKDPNEKRDHMVLLEFVTAAGITLGMDELYK*MYPYDVPDYAGYPYD*
VPDYAGYPYDVPDYA

Table S6. Complete nucleotide sequence of *Cyanidioschyzon merolae* codon-optimized *mCerulean3* with the sequence for a peroxisomal targeting signal 1 (PTS1). The PTS1 sequence is shown in blue.

ATGGTGTCGAAGGGCGAGGAGCTGTTCACGGGCGTGGTGCCGATCCTGGTGGAGCT
GGACGGCGACGTGAACGGCCACAAGTTCTCGGTGTCGGGTGAGGGCGAGGGTGACG
CGACGTACGGCAAGCTGACGCTGAAGTTCATCTGCACGACGGGCAAGCTGCCGGTGC
CGTGGCCGACGCTGGTGACGACGCTGTCGTGGGGCGTGCAGTGCTTCGCGCGCTAC
CCGGACCACATGAAGCAGCACGACTTCTTCAAGTCGGCGATGCCGGAGGGCTACGTG
CAGGAGCGCACGATCTTCTTCAAGGACGACGGCAACTACAAGACGCGCGCGGAGGTG
AAGTTCGAGGGCGACACGCTGGTGAACCGCATCGAGCTGAAGGGCATCGACTTCAAG
GAGGACGGCAACATCCTGGGCCACAAGCTGGAGTACAACGCGATCCACGGCAACGTG
TACATCACGGCGGACAAGCAGAAGAACGGCATCAAGGCGAACTTCGGCCTGAACTGC
AACATCGAGGACGGCTCGGTGCAGCTGGCGGACCACTACCAGCAGAACACGCCGATC
GGCGACGGCCCGGTGCTGCTGCCGGACAACCACTACCTGTCGACGCAGTCGAAGCT
GTCGAAGGACCCGAACGAGAAGCGCGACCACATGGTGCTGCTGGAGTTCGTGACGG
CGGCGGGCATCACGCTGGGCATGGACGAGCTGTACAAGTCGAAGCTG